



UNIVERSITÀ
DEGLI STUDI
FIRENZE

FLORE

Repository istituzionale dell'Università degli Studi di Firenze

Interfering with HuR-RNA Interaction: Design, Synthesis and Biological Characterization of Tanshinone Mimics as Novel, Effective

Questa è la Versione finale referata (Post print/Accepted manuscript) della seguente pubblicazione:

Original Citation:

Interfering with HuR-RNA Interaction: Design, Synthesis and Biological Characterization of Tanshinone Mimics as Novel, Effective HuR Inhibitors / Manzoni, Leonardo; Zucal, Chiara; Maio, Danilo Di; D'Agostino, Vito G.; Thongon, Natthakan; Bonomo, Isabelle; Lal, Preet; Miceli, Marco; Baj, Vanessa; Brambilla, Marta; Cerofolini, Linda; Elezgarai, Saioa; Biasini, Emiliano; Luchinat, Claudio; Novellino, Ettore; Fragai, Marco; Marinelli, Luciana*; Provenzani, Alessandro; Seneci, Pierfausto. - In: JOURNAL OF MEDICINAL CHEMISTRY. -

Availability:

This version is available at: 2158/1117511 since: 2021-03-23T18:13:59Z

Published version:

DOI: 10.1021/acs.jmedchem.7b01176

Terms of use:

Open Access

La pubblicazione è resa disponibile sotto le norme e i termini della licenza di deposito, secondo quanto stabilito dalla Policy per l'accesso aperto dell'Università degli Studi di Firenze (<https://www.sba.unifi.it/upload/policy-oa-2016-1.pdf>)

Publisher copyright claim:

(Article begins on next page)

Interfering with HuR-RNA Interaction: Design, Synthesis and Biological Characterization of Aza-tanshinones as novel, effective HuR Inhibitors

*Leonardo Manzoni,¹⁺ Chiara Zucal,²⁺ Danilo Di Maio,³⁺ Vito G.
D'Agostino,² Natthakan Thongon,² Isabelle Bonomo,² Preet Lal,² Marco
Miceli,⁴ Vanessa Baj,⁴ Marta Brambilla,⁴ Linda Cerofolini,^{5,6} Saioa
Elezgarai,⁷ Emiliano Biasini,^{2,7} Claudio Luchinat,⁶ Ettore Novellino,⁸ Marco
Fragai,^{5,6} Luciana Marinelli,^{8*} Alessandro Provenzani,^{2*} and Pierfausto
Seneci^{1*}*

¹Institute of Molecular Science and Technology (ISTM), CNR, Via Golgi 19, 20133 Milan, Italy

²Centre for Integrative Biology (CIBIO), University of Trento, Via Sommarive 9, 38123 Povo (TN), Italy

³Scuola Normale Superiore, Piazza dei Cavalieri 7, I-56126 Pisa, Italy.

⁴Chemistry Department, University of Milan, Via Golgi 19, 20133 Milan, Italy

⁵ Consorzio Interuniversitario di Risonanze Magnetiche di Metallo Proteine (CIRMMP), Via L. Sacconi 6, 50019 Sesto Fiorentino (FI), Italy

⁶ CERM and Chemistry Department, University of Florence, Via della Lastruccia 3-13, 50019 Sesto Fiorentino (FI), Italy

⁷ Istituto di Ricerche Farmacologiche Mario Negri, Milan, 20156, Italy

⁸ Pharmacy Department, University of Naples, Via Montesano 49, 80131 Naples, Italy

* To whom correspondence should be addressed:

Pierfausto Seneci Tel: +39 02-50314060; Fax: +39 02-50314074; pierfausto.seneci@unimi.it

Correspondence may also be addressed to:

Luciana Marinelli Tel: +39 081-679899; Fax: +39 081 676569; lmarinel@unina.it

Alessandro Provenzani Tel: +390461283176; Fax: +390461283239; alessandro.provenzani@unitn.it

+ The authors wish it to be known that, in their opinion, the first 3 authors should be regarded as joint First Authors

ABSTRACT:

The human antigen R (HuR) is an RNA-binding protein known to regulate cellular response to proliferation, differentiation, senescence, inflammation and immune-response. We previously found that Dihydrotanshinone-I (DHTS, **1**) prevents the association of HuR with its RNA substrate both *in vitro* and *in cell*. Herein, inspired by DHTS structure, we designed and synthesized an array of orto-quinones (aza-tanshinones) using a function-oriented synthetic approach. Among others, compound **6a** and **6n** turned out to be more effective inhibitors than **1**, showing a nanomolar K_i . A combined approach of NMR titration and Molecular Dynamic simulations suggest a possible mechanism of action for **6a**. Alpha screen and RNA-Electrophoretic mobility shift assays (REMSA) data on newly synthesized compounds allowed the generation of structure activity relationships (SARs), thus providing new insights about the HuR steric and electrostatic requirements. Ribonucleoprotein immunoprecipitation experiments showed that aza-tanshinones modulate HuR binding to important target mRNA such as VEGF, HER2 and β -catenin.

INTRODUCTION

The Human antigen R (HuR), also known as HuA or ELAVL1, is an ubiquitously expressed RNA binding protein that binds preferentially to adenine- and uridine-rich elements (ARE) of target coding and non-coding RNAs¹⁻³. HuR is primarily localized in the nucleus, where it exerts post-transcriptional functions such as splicing^{4,5} and alternative polyadenylation⁶, although it shuttles to the cytoplasm carrying the targeted RNA to be spatio-temporally regulated in translation and stability⁷. As a stress-response protein, HuR modulates the expression of target mRNA (containing AREs preferentially in their 3'UTR) coding for proteins involved in inflammation⁸, cell division⁹, tumorigenesis^{10,11}, angiogenesis^{12,13}, metastasis¹⁴, senescence¹⁵, apoptosis^{16,17}, immune^{18,19} or stress responses²⁰. The importance of HuR in inflammation and cancer has encouraged the search for inhibitors/modulators to interfere with its biological activity²¹. Several compounds have been named as HuR disruptors, i.e. molecules that can inhibit the HuR-RNA complex formation. Some examples were very recently reviewed²². However, neither systematic Structure-Activity Relationships (SARs) studies, nor chemical synthesis of novel families of HuR inhibitors have been reported so far. From a structural point of view, rational design of HuR inhibitors is rather challenging due to the protein conformational plasticity²³. Moreover, HuR switches between at least two conformations upon binding/unbinding of its RNA substrate: an “open” (apo) conformation, which is characterized by almost no contacts between its first two RNA recognition motif (RRM) domains, and a “closed” (holo) conformation, which is instead characterized by a few inter-residue contacts between the RRM domains. Recently, as a result of a high throughput screening on a set of anti-inflammatory agents, we identified Dihydrotanshinone-I (**1**, DHTS, Figure 1), a low molecular weight natural product able to interact with HuR, thus affecting its post-transcriptional functions²⁴. **1** is a major component of extracts from Danshen (*Salvia miltiorrhiza*) used in traditional Chinese medicine as a treatment for inflammation, cardiovascular and cerebrovascular

diseases ²⁵. Our detailed *in vitro* and *in vivo* characterization of DHTS showed the HuR dependency of its mechanism of action ²⁴ and its potency on cancer-connected HuR-mRNA interactions ¹¹. Naturally occurring tanshinones **2-4** (Figure 1) were tested as HuR inhibitors, observing a preference for an aryl condensed (compounds **1-2**) vs. saturated D rings (compounds **3-4**)²⁴.

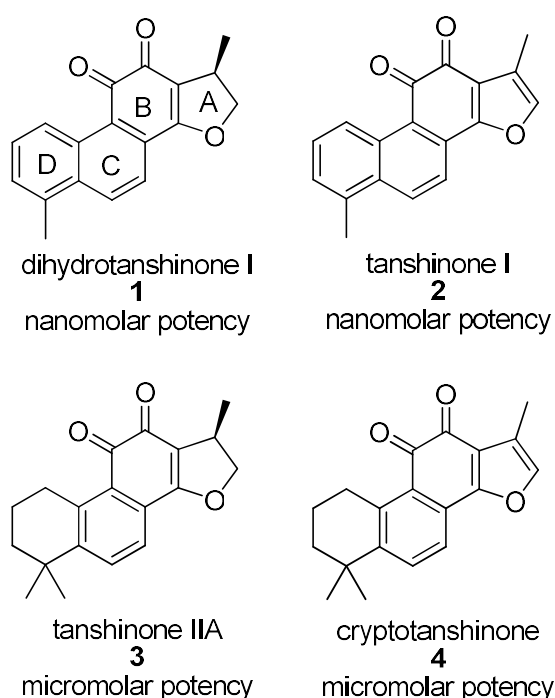


Figure 1. Naturally occurring tanshinones **1-4**.

Structural complexity has long hindered the synthetic exploitation of natural products as drug-oriented chemotypes. However, molecular editing through diverted total synthesis ²⁶ and function-oriented synthesis (FOS) ²⁷ are synthetic paths that help to transform a natural product to a simpler, equally active synthetic analogue ²⁸.

We applied a FOS approach to DHTS, starting from the bicyclic A-B scaffold **5** (Figure 2). It contains the o-quinone group and a pyrrole A ring, to provide novel, DHTS-inspired, synthetic *aza-tanshinones* bearing R₁-R₄ substitutions. Here the synthesis of a small library of aza-tanshinones **6a-t**,

bearing substitutions in positions 1, 3, 6 and 7, is reported. Aza-tanshinones were tested for inhibition of HuR-RNA interactions, and SARs were established. The most potent HuR inhibitor **6a** (Figure 2) was further characterized in a panel of *in vitro* and cellular assays and showed a direct K_d of 4.5 μM to HuR. The molecular interaction of **6a** with HuR, and with the HuR-mRNA complex was also elucidated *via* a combined approach of NMR and computational studies and grounded the path for the next generation of HuR inhibitors.

RESULTS AND DISCUSSION

Synthesis

Retrosynthesis. A FOS-based approach to natural products analogues entails the design of an uncomplicated synthetic strategy towards equally active, significantly simpler compounds. We built our strategy around a B ring-like ortoquinone, and we opted for a substituted, N-sulfonylated bicyclic A-B scaffold **6** as a function-oriented replacement for the tanshinone A-D ring system. The furan-pyrrole A ring switch was meant to provide HuR inhibition-inspired novelty, as the N-substituted indole MPT0B098 (**7**, Figure 2) is a negative modulator of HuR²⁹.

We reasoned that a preliminary SAR around positions 1, 3, 6 and 7 on scaffold **6** could be established by exploiting N-sulfonylations (functionalization of N-1, -SO₂R₁), Suzuki couplings (functionalization of C-3, -R₂), radical CH functionalizations³⁰ and Michael additions (functionalization of C-7, -R₃) and Diels-Alder cycloadditions (functionalization of C-6 and C-7, -cycloR₃-R₄, Figure 2).

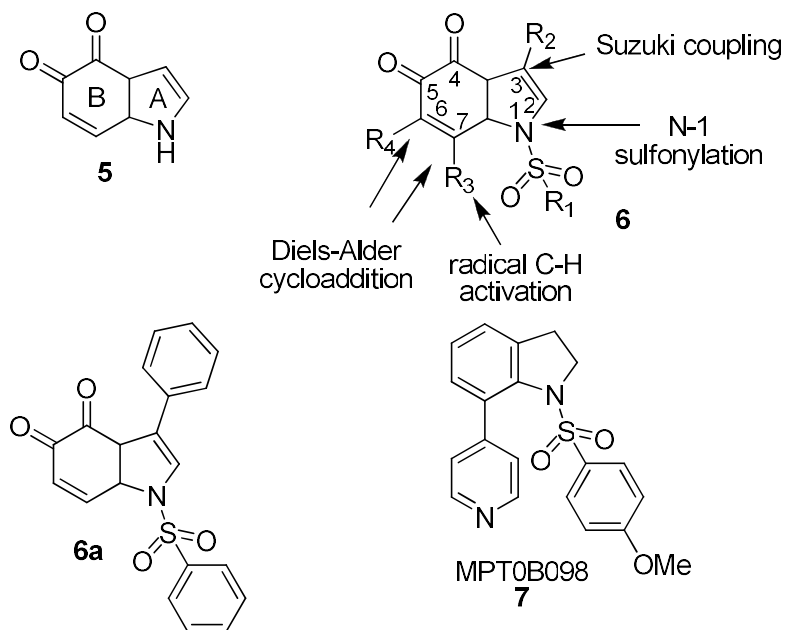
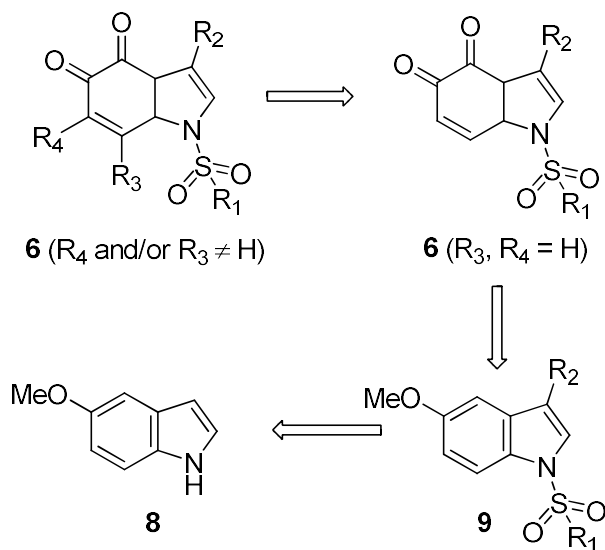


Figure 2. Aza-tanshinones as HuR inhibitors: core scaffold, function-oriented synthesis, active analogues.

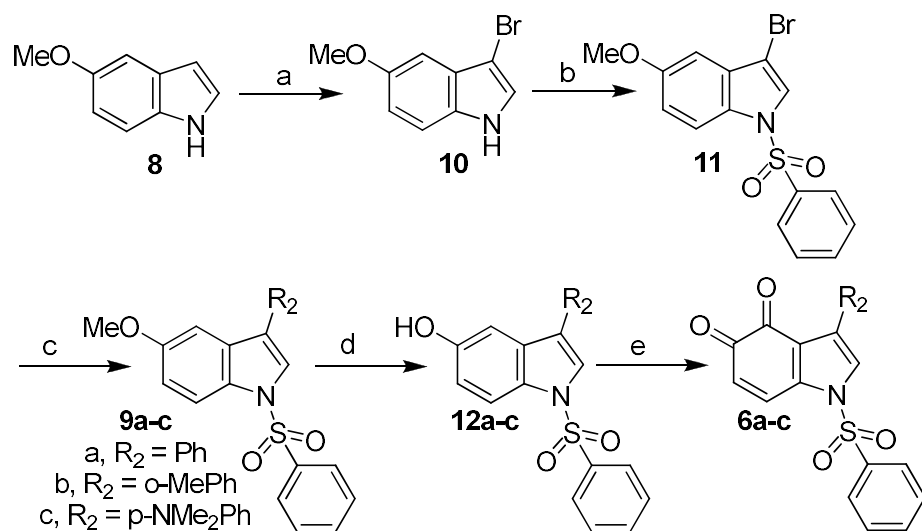
As to synthetic targets **6** (R_1 , R_2 , $R_4 \neq H$, or $R_1 - R_4 \neq H$, Scheme 1), we envisaged that functionalization of C-6 and/or C-7 could be carried out on 1,3-disubstituted indole-4,5-diones **6** (R_3 , $R_4 = H$). Such compounds could be made by O-demethylation and oxidation of 1,3-disubstituted 5-methoxyindoles **9**. Compounds **9** could be prepared by 3-bromination of commercially available 5-methoxyindole **8**, followed by N-sulfonylation and Suzuki coupling (Scheme 1).



Scheme 1. Retrosynthetic analysis to aza-tanshinones **6**.

1-Alkyl/Arylsulfonyl-3-Aryl Indole-4,5-Diones 6a-6j. The retrosynthetic scheme leading to 1,3-disubstituted indole-4,5-diones **6** ($\text{R}_1, \text{R}_2 \neq \text{H}$, $\text{R}_3 = \text{R}_4 = \text{H}$, Figure 1) was validated by synthesizing 1-phenylsulfonyl-3-phenyl indole-4,5-dione **6a** (Scheme 2). 5-Methoxyindole **8** was brominated in position 3 (step a, compound **10**) and treated with phenylsulfonyl chloride (step b). 3-Bromo phenylsulfonamide **11** was reacted with phenyl boronic acid in a Suzuki coupling (step c) to provide, after careful optimization of the experimental protocol, to 1-phenylsulfonyl-3-phenyl-5-methoxyindole **9a**. Demethylation (step d, compound **12a**) and oxidation with IBX³¹ (step e) led to 1-phenylsulfonyl-3-phenyl indole-4,5-dione **6a** (Scheme 2) with an overall $\approx 35\%$ yield.

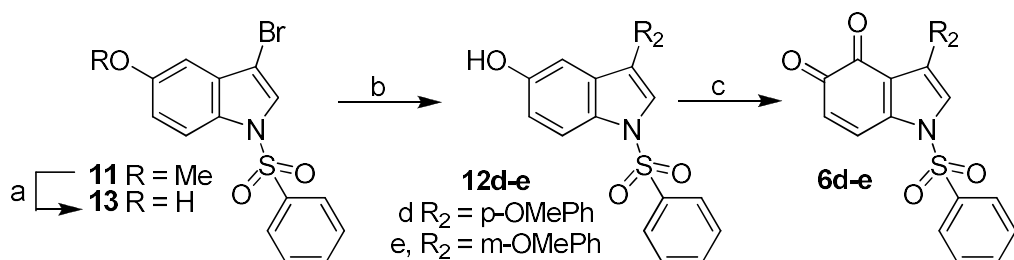
3-Bromo phenylsulfonamide **11** was reacted with *o*- ($\text{R}_2 = o\text{-MePh}$, **9b**) and *p*-substituted phenyl boronic acid ($\text{R}_2 = p\text{-NMe}_2\text{Ph}$, **9c**) (step c), and respectively converted to 1-phenylsulfonyl-3-*o*-methylphenyl indole-4,5-dione **6b** and 1-phenylsulfonyl-3-*p*-dimethylaminophenyl indole-4,5-dione **6c** (steps d,e, Scheme 2) as reported for **6a**.



Scheme 2. Synthesis of 1-phenylsulfonyl-3-aryl indole-4,5-diones **6a-c**.

Reagents and conditions: (a) Br_2 , DMF, rt, 24 hrs, 74%; (b) PhSO_2Cl , $\text{n-Bu}_4\text{N}^+\text{HSO}_4^-$, aqueous 50% KOH, CH_2Cl_2 , rt, 3 hrs, 90%; (c) arylboronic acid, $\text{Pd(PPh}_3)_4$, dry DME/EtOH 4/1, N_2 atmosphere, rt, reflux, 8 hrs, 83-92%; (d) 1M BBr_3 in dry CH_2Cl_2 , N_2 atmosphere, -78°C to 5°C , 87-99%; (e) IBX, EtOAc (40°C) or DMF (rt), 2 to 24 hrs, 87-96%.

The synthesis of *p*-substituted ($\text{R}_2 = \text{p-OMe}$, **9d**) and *m*-substituted ($\text{R}_2 = \text{m-OMe}$, **9e**) aryl ethers (Scheme 3) required demethylation of the 5-methoxy group on 3-bromo phenylsulfonamide **11** (step a) before Suzuki coupling (step b) and IBX oxidation (step c, Scheme 3) to avoid undesired demethylation of the 3-*m*- or *p*-methoxyphenyl group.

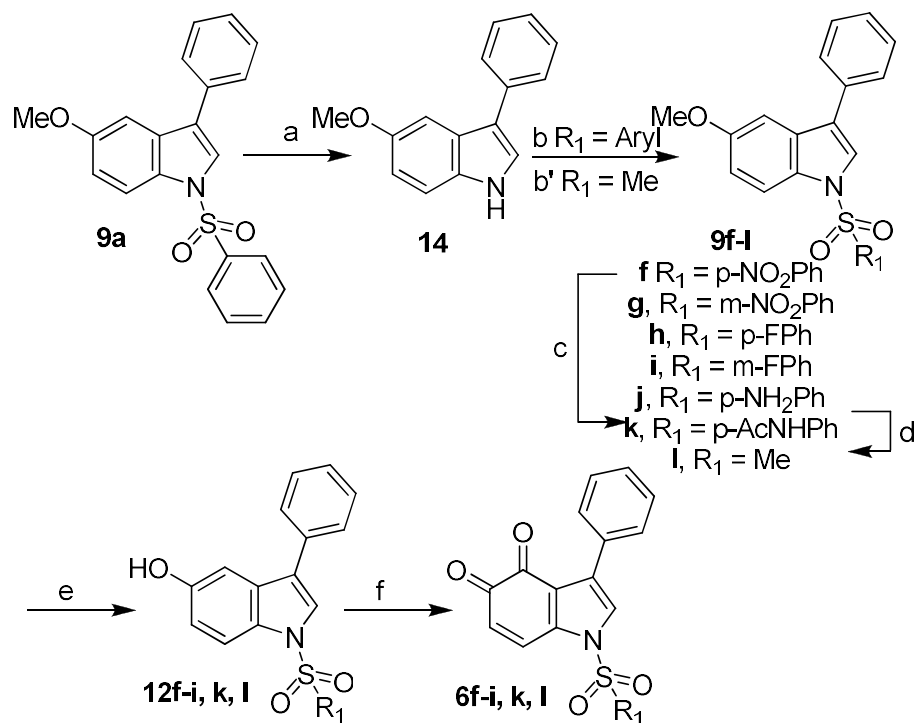


Scheme 3. Synthesis of 1-phenylsulfonyl-3-methoxyphenyl indole-4,5-diones **6d,e**.

Reagents and conditions: (a) 1M BBr₃ in dry CH₂Cl₂, N₂ atmosphere, -78°C to 5°C, 86%; (b) methoxyphenylboronic acid, Pd(PPh₃)₄, dry DME/EtOH 4/1, N₂ atmosphere, rt, reflux, 8 hrs, 79-85%; (c) IBX, DMF, rt, 6 to 48 hrs, 67-87%.

We attempted the synthesis of 1-alkylsulfonyl or 1-*m/p*-substituted arylsulfonyl-3-phenyl indole-4,5-diones **6f-l** by replacing phenylsulfonyl chloride with alkyl- or *m/p*-aryl sulfonyl chlorides (Scheme 2). Unfortunately, the Suzuki coupling protocol optimized for the synthesis of **9a** was not applicable as such to other sulfonamides. Thus, we synthesized compounds **6f-i,k,l** according to the longer, more efficient strategy depicted in Scheme 4.

1-Phenylsulfonyl-3-phenyl-5-methoxyindole **9a** was de-sulfonylated (step a, compound **14**) and treated with aryl- (step b) or alkylsulfonamides (step b') to provide 1-*m/p*-substituted arylsulfonyl- and 1-methylsulfonyl-3-phenyl-5-methoxy indoles (respectively **9f-i** and **9l**) in good to excellent yields. 1-*p*-Nitrophenylsulfonyl-3-phenyl-5-methoxyindole **9f** was reduced (step c, amine **9j**) and acetylated to 1-*p*-acetamidophenylsulfonyl-3-phenyl-5-methoxyindole **9k** (step d). Conversion of aryl ethers **9f-i,k,l** into 1-*m/p*-substituted arylsulfonyl- or 1-alkylsulfonyl-3-phenyl indole-4,5-diones **6f-i,k,l** (steps e and f, Scheme 4) was carried out as previously described for **6a**.

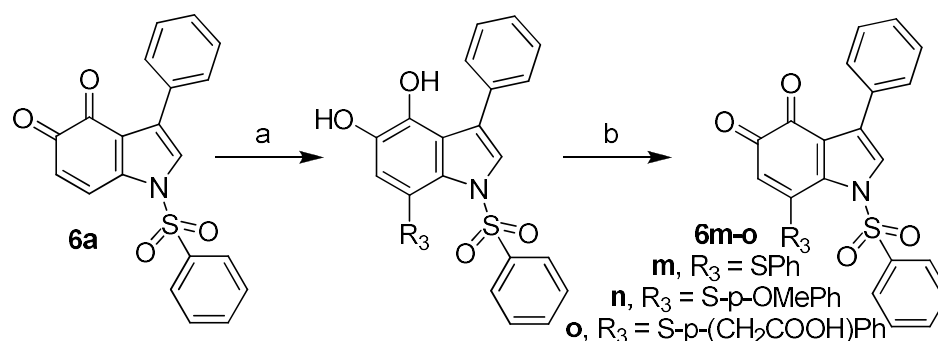


Scheme 4. Synthesis of 1-alkyl/arylsulfonyl-3-phenyl indole-4,5-diones **6f-i,k,l**.

Reagents and conditions: (a) Aqueous 3M NaOH, 2/1 MeOH/THF, 80°C, 2 hrs, 98%; (b) R₁SO₂Cl, n-Bu₄N⁺HSO₄⁻, 50% KOH, CH₂Cl₂, rt, 3 hrs, 87-92%; (b') NaH, mesyl chloride, dry DMF, N₂ atmosphere, 0°C to rt, 3 hrs, 59%; (c); SnCl₂·2H₂O, 1/1 THF/MeOH, 80°C, 2hrs, 95%; (d); Ac₂O, pyridine, CH₂Cl₂, rt, 22 hrs, 82%; (e) 1M BBr₃ in dry CH₂Cl₂, N₂ atmosphere, -78°C to 5°C, 73-99%; (f) IBX, EtOAc (40°C) or DMF (rt), 2 to 24 hrs, 87-96%.

1-Phenylsulfonyl-3-Phenyl-7-Thioaryl Indole-4,5-Diones 6m-6o. The retrosynthetic scheme leading to 1,3,7-trisubstituted indole-4,5-diones **6** (R₁, R₂ ≠ H, R₃ = S-Ar, R₄ = H, Figure 2) was validated by synthesizing 1-phenylsulfonyl-3-phenyl-7-thiophenylindole-4,5-dione **6m** (Scheme 5) *via* Michael addition of substituted benzenethiols on *o*-quinones³¹. Namely, 1-phenylsulfonyl-3-phenyl indole-4,5-dione **6a** was treated with thiophenol (step a), providing 1-phenylsulfonyl-3-phenyl-7-thiophenylindole-

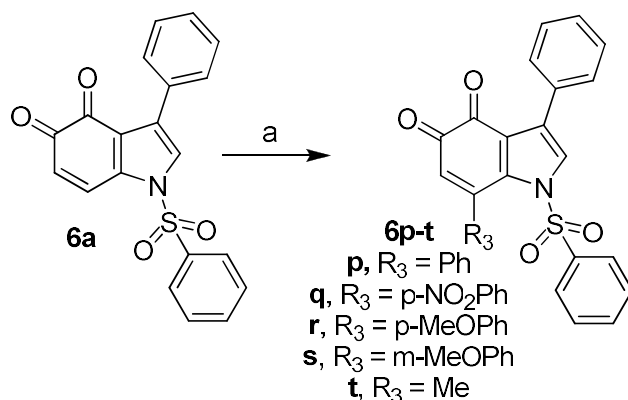
4,5-dione **6m** after oxidation of the reduced form(step b, Scheme 5) in moderate yield after extensive optimization. The optimized experimental protocol was used with p-methoxybenzenethiol (**6n**) and p-carboxymethylbenzenethiol (**6o**), observing moderate two step yields for both quinones.



Scheme 5. Synthesis of 1-phenylsulfonyl-3-phenyl-7-thioaryl indole-4,5-diones **6m-6o**.

Reagents and conditions: (a) aryl thiol, DMF, 2-3 hrs, rt, 62-88%; (b) IBX, DMF, 2 hrs, rt, 52-56%.

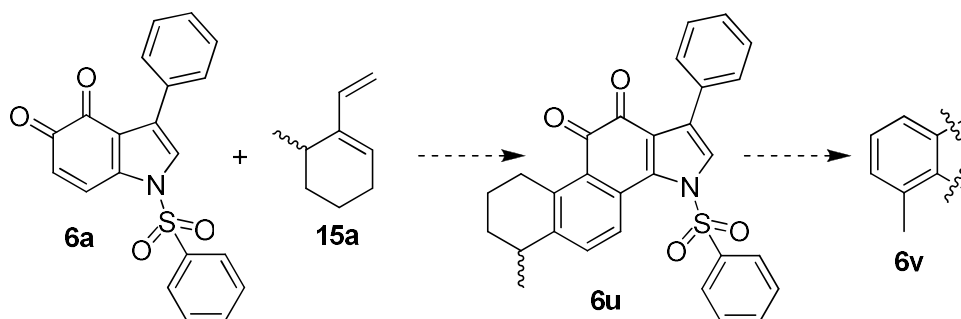
1-Phenylsulfonyl-3-Phenyl-7-Aryl Indole-4,5-Diones 6p-6t. The retrosynthetic scheme leading to 1,3,7-trisubstituted indole-4,5-diones **6** ($\text{R}_1, \text{R}_2, \text{R}_3 \neq \text{H}, \text{R}_4 = \text{H}$, Figure 1) was validated by synthesizing 1-phenylsulfonyl-3,7-diphenylindole-4,5-dione **6p** (Scheme 6) *via* Mn(III)-mediated radical addition of boronic acids^{30,32}. 1-Phenylsulfonyl-3-phenyl indole-4,5-dione **6a** was treated with phenylboronic acid and $\text{Mn}(\text{OAc})_3$ (step a), providing 1-phenylsulfonyl-3,7-diphenylindole-4,5-dione **6p** (Scheme 6). The experimental protocol required extensive optimization, and a moderate yield was finally obtained. The optimized experimental protocol was then used with aryl- (**6q-s**) and alkylboronic acids (**6t**), adapting the reaction time to each substrate (Scheme 5) and observing poor to moderate reaction yields.



Scheme 6. Synthesis of 1-phenylsulfonyl-3-phenyl-7-aryl indole-4,5-diones **6p-6t**.

Reagents and conditions: (a) boronic acid, $\text{Mn}(\text{OAc})_3$, 1,2-dichloroethane, 80°C , 30 to 150 minutes, 14-36%.

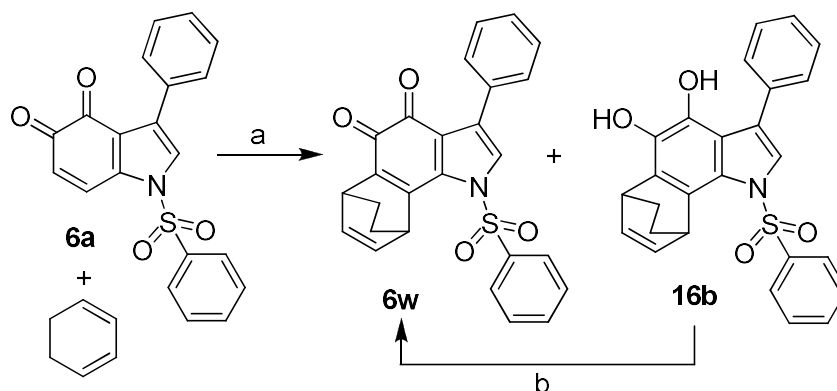
Diels-Alder Cycloadducts 6u-6w. Validation of the retrosynthetic scheme to 1,3,6,7-tetrasubstituted indole-4,5-diones **6** ($\text{R}_1, \text{R}_2 \neq \text{H}$, cyclo R_3R_4 , Figure 1) targeted 1-phenyl-3-phenylsulfonyl-6-methylphenantro[1,2-b]pyrrole-10,11-dione **6v**. We envisaged a Diels-Alder cycloaddition between 1-phenylsulfonyl-3-phenyl indole-4,5-dione **6a** and 6-methyl-1-vinylcyclohexene **15a**, followed by DDQ dehydrogenation/aromatization of tetrahydrocycloadduct **6u** to aromatic **6v** (Scheme 7) ³³. Unfortunately, we could not obtain pure **15a** in reasonable amounts following the published synthetic procedure ³³



Scheme 7. Attempted synthesis of 6,7,8,9-tetrahydro-1-phenyl-3-phenylsulfonyl-phenanthro[1,2-b]indole-10,11-dione **6v**.

Due to the inhibitory activity observed with bicyclic indole-4,5-dione **6a** and some of its congeners, a tetracyclic, tanshinone-like core should not be necessarily needed to prevent HuR-mRNA interactions. Thus, cycloadditions on dienophile **6a** were targeted to introduce potency-oriented (additional interactions with the binding site on HuR) and/or “druggability”-oriented substitutions on C-6 and C-7 (modulation of selectivity, solubility and lipophilicity, etc.).

Diels-Alder cycloaddition between 1,3-cyclohexadiene **15b** and dienophile **6a** provided a mixture of desired *orto*-quinone **6w** and diphenol **16b** (step a, Scheme 8). Oxidation (step b) converted the mixture to pure **6w**.



Scheme 8. Synthesis of cycloadduct **6w**.

Reagents and conditions: (a) Cat. dry ZnCl_2 , dry CH_2Cl_2 , Ar atmosphere, 0°C , 5 min, 88%; (b) CAN, 2/1 MeCN/ H_2O , 0°C , 10 min, quantitative.

A more systematic effort towards tanshinone-like 1,3,6,7-tetrasubstituted indole-4,5-diones **6** (R_1 , $\text{R}_2 \neq \text{H}$, cyclo R_3R_4 , Figure 1) will be carried out, and reported in future.

Biochemical characterization

6a and **6n**, are more effective than DHTS in inhibiting the HuR-RNA complex formation. Aza-tanshinones **6a-i**, **6k-t** and **6w** were evaluated using a previously developed biochemical tool based on Amplified Luminescent Proximity Homogenous Assay Alpha-Screen technology^{24,34}. Recombinant His-tagged HuR (rHuR) bound to nickel chelate acceptor beads, was incubated with a biotinylated single strand AU-rich RNA probe (Bi-AU), recognized by streptavidin-coated donor beads. When rHuR binds to the Bi-AU, the beads are brought into proximity and a fluorescence signal can be detected. We evaluated the ability of aza-tanshinones to inhibit the rHuR-Bi-AU complex formation in saturation binding conditions. Knowing that the K_d value for the rHuR-Bi-AU interaction is 2.5 nM ²⁴, we fitted on AlphaScreen saturation curves the K_i values, quantifying the inhibitory efficiency of tested compounds from high to low nanomolar range (Table 1, mid column). Among aza-tanshinones showing K_i with a percentage of % inhibition $>50\%$, compound **6a** ($K_i = 12.8 \text{ nM}$) and **6n** ($K_i = 15 \text{ nM}$) were more effective than DHTS (**1**), while compounds **6h**, **6k**, **6l**, **6r** and **6s** showed similar activity (Figure 3 and Table 1).

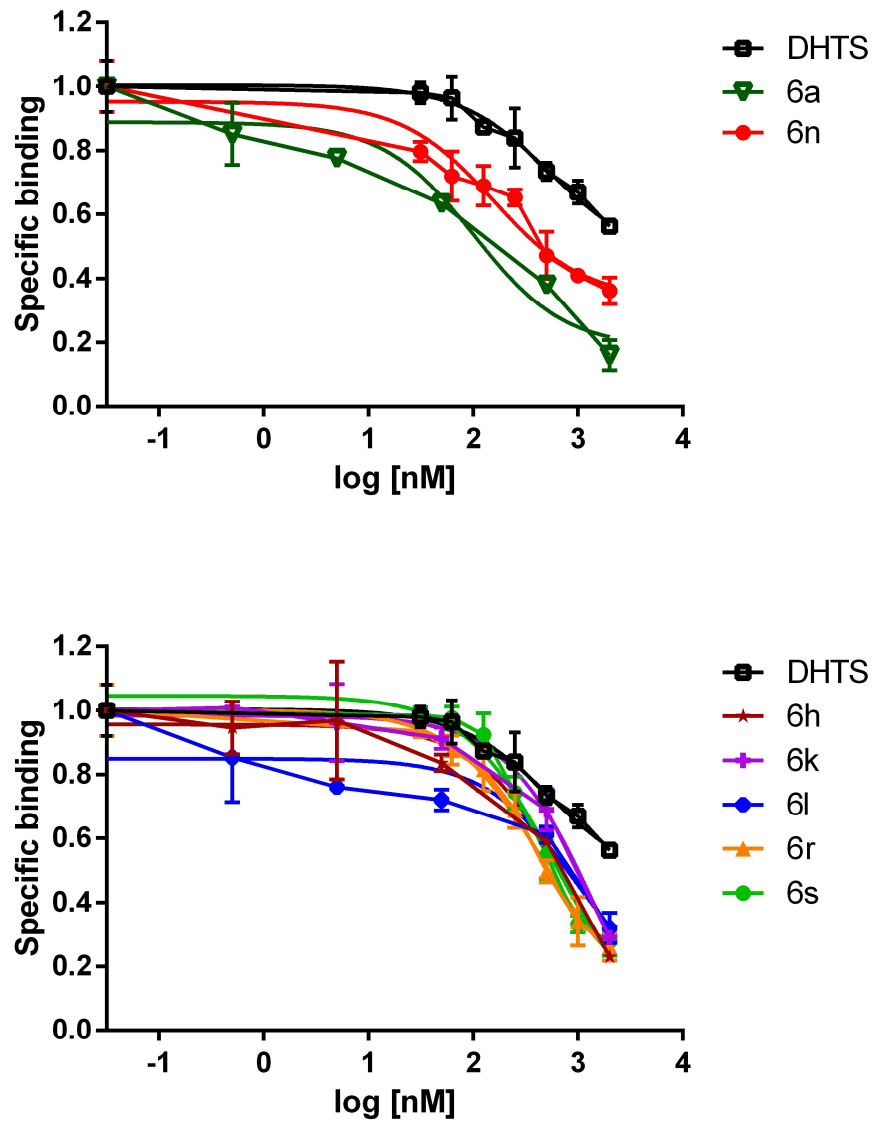


Figure 3. K_i calculation by Alpha screen assessing specific binding of His-tagged HuR and the AU-rich biotinylated RNA. K_i were calculated with respect to a K_d of 2.5 nM for the rHuR-Bi-AU interaction, and normalized to control (DMSO). Fitting curves show nonlinear regression fits of the data according to a 1-site binding model in GraphPad Prism. Plotted bars are mean \pm SD of two independent experiments.

Table 1

Compound	Ki, nM
1/DHTS	50
6a	12.8
6b	Interfering
6c	>100
6d	>200
6e	>200
6f	Interfering
6g	>100
6h	48
6i	>100
6k	81
6l	56
6m	Interfering
6n	15
6o	Interfering
6p	>100
6q	>100
6r	41
6s	55
6t	>200
6w	>300

Aza-tanshinones **6b**, **6f**, **6m** and **6o** resulted as interferers in AlphaScreen³⁵, thus we proceeded with a second independent, orthogonal assay protocol for these and a few other aza-tanshinones (Figure 4 and Supporting Figures 1 and 2). We evaluated their inhibitory ability *via* a non-denaturing and non-

crosslinked REMSA^{24,34}. After mixing at least 10 fold excess of rHuR with 50 fmol of 5'-DY681-labeled AU-rich RNA probe (DY681-AU) or with 25 nM of FAM-RNA probe, we observed the formation of the higher, oligomeric molecular weight complex between protein and RNA. The concomitant addition of active aza-tanshinones (5 μ M concentration) caused a reduction of the shifted RNA probe, allowing qualitative estimation of their inhibitory ability towards the Bi-AU ligand at equilibrium. We noticed a concordance between the two biochemical assays for compounds **6a**, **6c**, **6k**, **6n**, **6p-6t** and **6w**. Aza-tanshinones **6b**, **6f**, **6m** and **6o** were therefore classified as inhibitors endowed with intermediate potency (Figure 4).

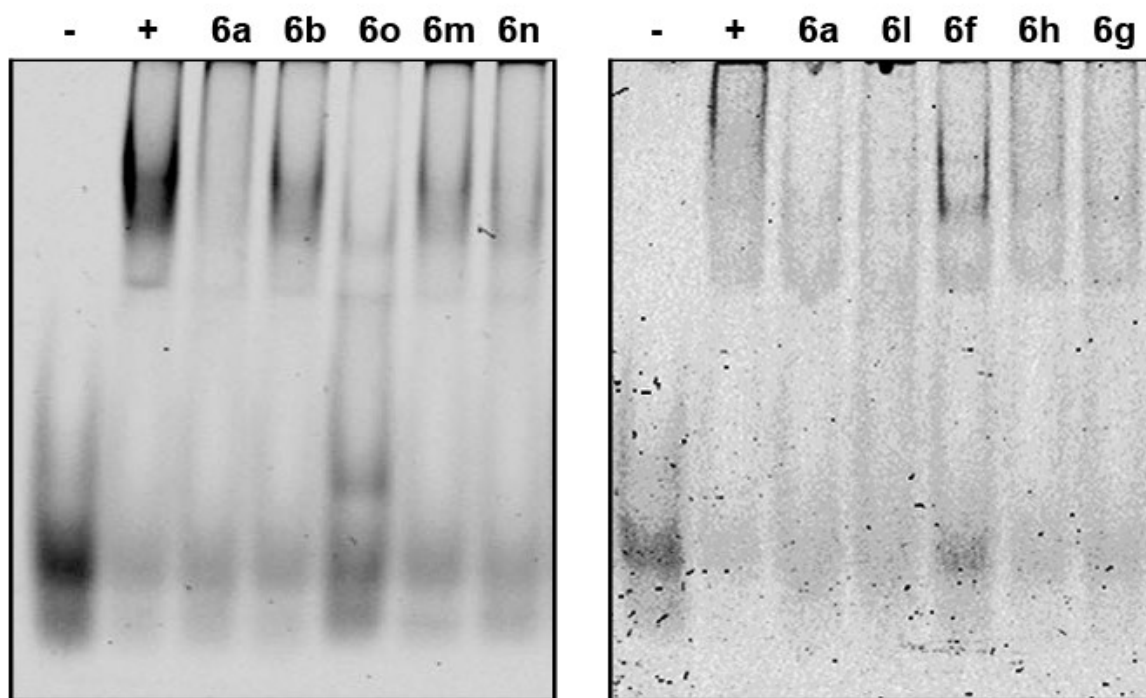


Figure 4. REMSA characterization on selected aza-tanshinones. REMSA assay performed with at least 10-fold excess of recombinant HuR incubated for 30 min with either 25 nM of 5'-FAM-labeled RNA probe (left) or with 50 fmol of 5'-DY681-labeled RNA probe (right). Incubation with RNA probe

only (-), with rHuR, RNA probe and DMSO (+) used as positive control of the binding, and incubation with aza-tanshinones **6** (5 μ M).

Aza-tanshinone 6a directly binds to HuR protein and modulates intracellular target mRNAs binding. Compound **6a** was selected among the most potent aza-tanshinones for further evaluation. It showed a similar mechanism to DHTS in preventing the association step with RNA probe ²⁴, as highlighted in dissociation experiments performed upon pre-incubation of protein and RNA (Figure 5).

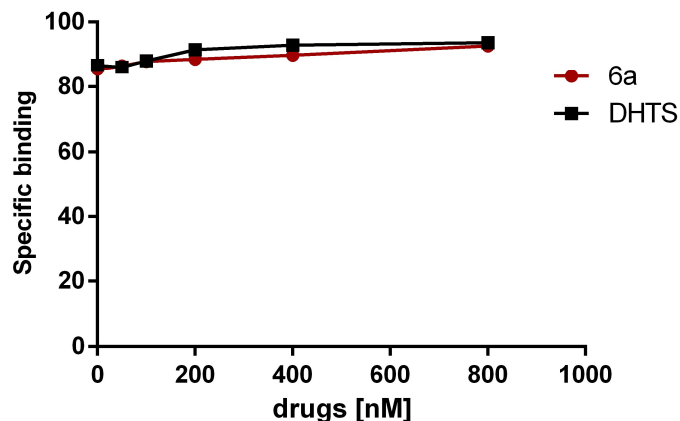


Figure 5. Dissociation experiments. Specific binding was evaluated by Alpha screen, performed upon 30 min pre-incubation of 1 nM of rHuR and 50 nM of biotinylated-RNA, before addition of DHTS or **6a** in the indicated doses. Mean \pm SD refers to three independent experiments.

Dynamic mass redistribution (DMR) analysis ³⁶revealed, in a label-free format, a direct protein:**6a** interaction at the equilibrium (Figure 6). rHuR, or its truncated form comprising the first two domains (RRM1-RRM2HuR), was immobilized onto the surface of label-free microplates by amine-coupling chemistry. Different amounts of **6a** (0.03-100 μ M) were added to the wells and the mass of molecular complexes was detected after a 30 min incubation. Dose-dependent binding of **6a** to

rHuRandRRM1-RRM2 HuR was observed in the 0.3-10 μ M range, sufficient to obtain saturation. The estimated affinity constant (K_d) was $\approx 4.5 \mu$ M, for both proteins. The same experiment was performed with DHTS, but it was impossible to evaluate the K_d due to its poor solubility ²⁴.

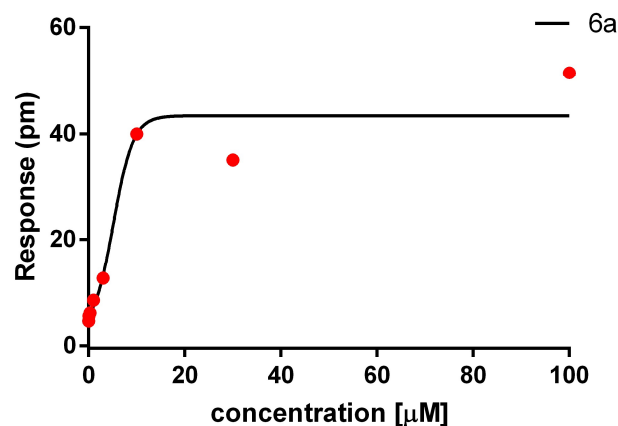
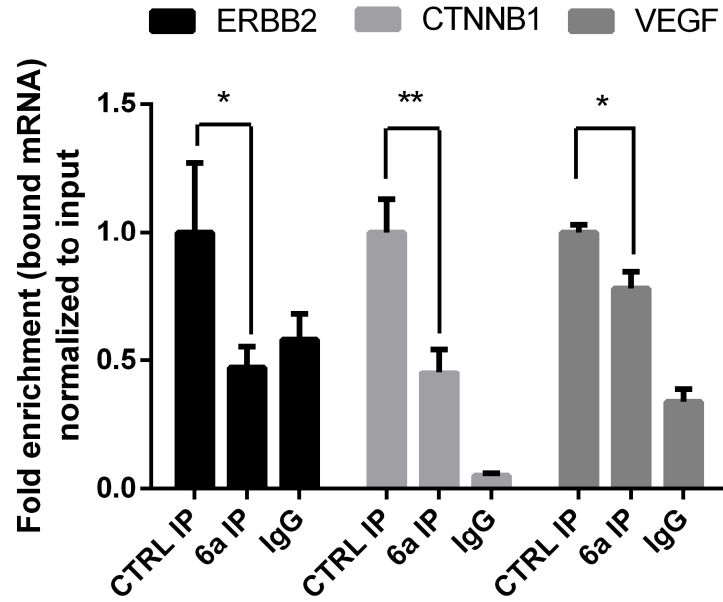


Figure 6.6a binds to recombinant HuR. Different concentrations of **6a** were added to label-free microplate wells on which aliquots of full-length or RRM1-RRM2HuR proteins had previously been immobilized. Measurements were performed before (baseline) and after (final) adding the compound. The response (pm) was obtained subtracting the baseline output from the final output signals. The output signal for each well was obtained by subtracting the signal of the protein-coated reference area from the signal of uncoated area. The data (red dots) were fitted (black line) to a sigmoidal function using a 4 parameter logistic (4PL) nonlinear regression model: $R^2 = 0.944$; $p = 0.009$.

We then determined if **6a** was interfering on HuR-RNA binding in MCF7 cells. We performed an RNA immunoprecipitation (RIP) assay ³⁷ on MCF7 extracts testing three validated HuR transcripts. We clearly observed either a subsequent decrease of to the relative number of mRNA copies and a decreased expression level of such mRNAs (Figure 7A, B). Therefore, compound **6a** directly binds to HuR both *in vitro* and *in cell*, in a region contained between the first two domains.



B

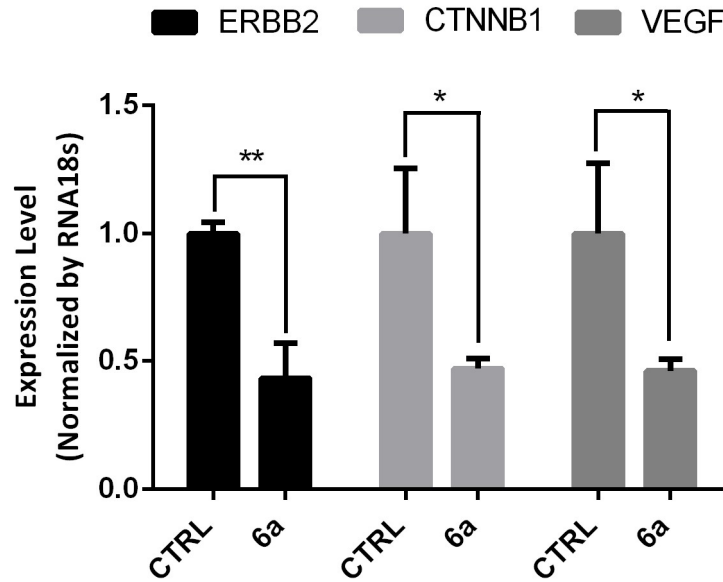


Figure 7. RNA immunoprecipitation (RIP) and quantitative real-time PCR (qRT-PCR). **A**). RIP was performed in MCF7 cells, lysed after 3h treatment with DMSO (CTRL) or **6a** (5 μ M). HuR antibody (IP) or an IgG isotype (IgG) were used for RNA precipitation. Changes in the mRNAs bound to immunoprecipitated HuR in the control or treatment condition were assessed by qRT PCR, and compared

with the ones obtained with IgG precipitation, used as negative control. All the relative values (Fold enrichment) were normalized to input, considering the value of the housekeeping gene RPLP0. **B)** MCF7 were treated with **6a** (5 μ M) for 6h to evaluate changes in total RNA levels. Expression level of *ERBB2*, *CTNNB1* and *VEGF* were measured by qRT-PCR and normalized to *RNA18s*. Data are presented as mean \pm SD of a biological triplicate (* $p < 0.05$ and ** $p < 0.01$ versus CTRL).

NMR and MD simulations.

Aza-tanshinone 6a blocks HuR in a “closed” conformation. The 2D ^1H - ^{15}N HSQC spectrum of RRM1-RRM2 domains showed well-dispersed signals in accordance with a folded protein structure, whose residues, including those of the linker region, have been previously assigned by us ³⁸. The resonances of residues forming the RRM1 domain are almost the same in the isolated domain ³⁹ and in the RRM1-RRM2 construct. The large superimposition of the signals in the isolated RRM1 and in the tandem domains is in agreement with the relaxation data that show as the two domains move independently in solution in the absence of RNA ³⁸. In line with the previously reported crystal structures of HuR, each domain in the RRM1-RRM2 construct is constituted by two α -helices and four β -strands ⁴⁰.

The molecular interaction of **6a** with RRM1-RRM2 tandem domains of HuR was evaluated through solution NMR ⁴¹. Compound **6a** shows improved solubility with respect to **1** ³⁸. Its effects on the protein is appreciable in the 2D ^1H - ^{15}N HSQC in the presence of 0.6 equivalents of the ligand, while with **1** comparable effects were observed after the addition of 4 equivalents. As also reported for **1** ³⁸, a generalized decrease in signal intensity was observed for the protein resonances, with few residues (Thr20, Leu22, Val66, Ser94, Tyr95, Ile103, Asn107, Leu108, Tyr109, Ile133, Val137, Leu138, Val139, Ser146) experiencing a stronger effect (Figure 8). Aza-tanshinone **6a** and **1** interact with the protein in the same region, i.e. the β -platform of both domains. In particular, eight amino acids (Thr20, Ser94,

Tyr95, Asn107, Leu108, Ile133, Val137, Leu138) experience a decrease in signal intensity with both ligands.

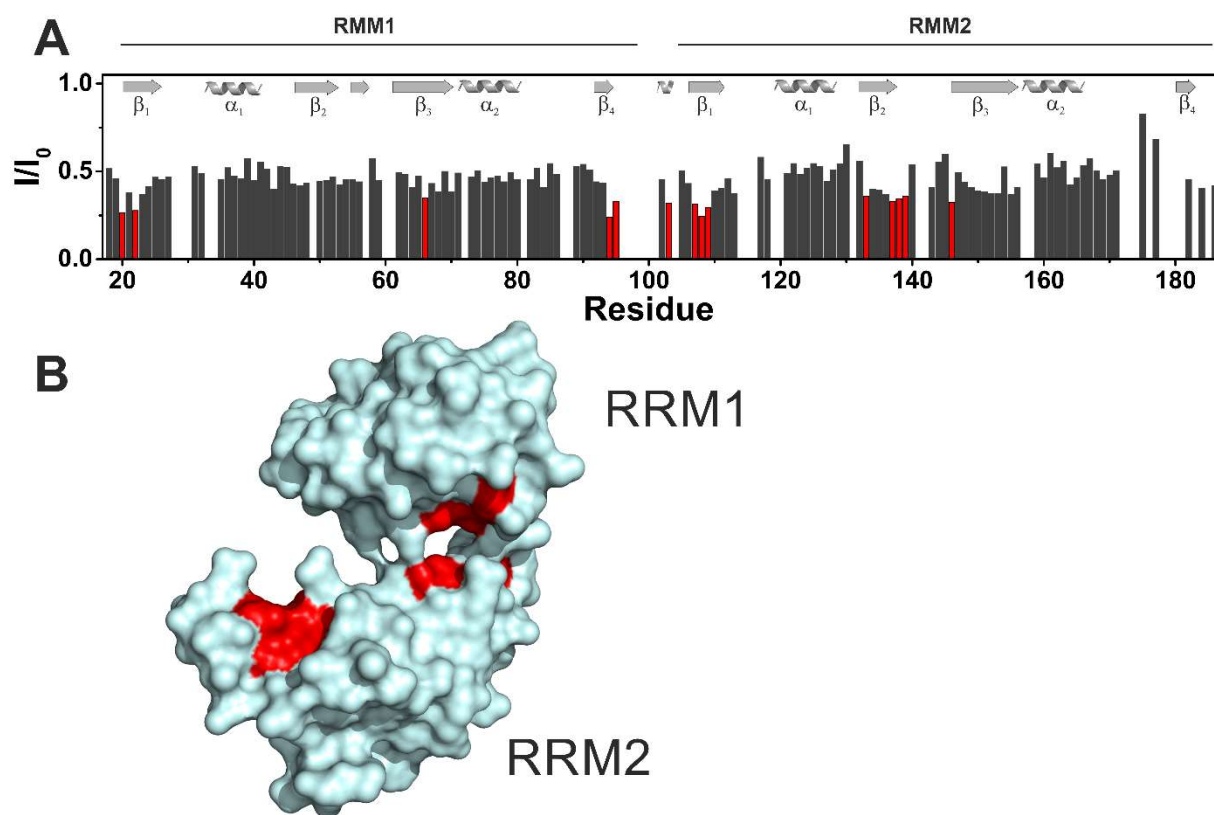


Figure 8. 6a stabilized recombinant HuR in a “closed” conformation. **A)** Graphical representation of the intensity changes of RRM1-RRM2 HuR protein per residues in the presence of 0.6 equivalents of **6a**. The residues exhibiting the highest decreases in signal intensities are colored in red. The secondary structures of the domains are reported on the graph. **B)** Surface representation of the closed (pdb: 4ED5) conformation of HuR. The residues exhibiting the largest decrease in signal intensities in the presence of 0.6 equivalents of **6a** are shown in red.

The generalized decrease of signal intensity, together with the distribution of affected residues over the large surfaces of the β -platform in each domain suggests an alteration of the equilibrium between “closed” and “open” conformations upon ligand binding. Specifically, the decrease of signal intensity was consistent with a mechanism where compound **6a** stabilizes a “closed” conformation of HuR. Collectively, NMR analysis indicates that **1** and **6a** bind the HuR protein approximately in the same region, producing similar effects on protein dynamics. However, it is interesting to note that one residue (Ile103) of the inter-domain linker (hereafter referred to as “hinge” loop) is sensitive to **6a** and not to **1**. This experimental evidence would suggest for **6a** a binding site in a more close proximity of the hinge loop, with respect to **1**. To better explore this possibility a molecular modeling study was performed.

To this purpose, a combined approach of docking calculations and extended molecular dynamics (MD) simulations was applied. Specifically, we first attempted a “blind” docking to the entire HuR surface, using two different docking softwares (AutoDock4.2 and Glide 6.5). Most of the highest-score poses of **6a** suggested by AutoDock were located within the RNA binding cleft (residues 18 to 95 of RRM1 and 107 to 185 of RRM2) and in proximity of the “hinge” loop. On the other hand, docking results with Glide converged towards one solution, which was different from those predicted by Autodock, though it was placed in proximity of the “hinge” loop as well. Therefore, albeit these results seem to indicate the region surrounding the “hinge” loop as the most likely binding region for **6a**, docking failed to unequivocally pinpoint one privileged binding mode, likely owing to omission of full receptor flexibility from the state-of-the-art docking softwares. To account for the missing receptor flexibility, we carried out multiple extended MD simulations on a reasonable number of **6a** binding modes, for a total simulation time of 6 μ s, and assessed their relative stability. Specifically, we opted for the binding pose predicted by Glide (Figure 9A) and the three best ranked and most diverse poses (in terms of root mean square deviation (RMSD) predicted by AutoDock (Figure 9B,C,D). In all four cases, **6a** drifted away from its starting docking position and explored a significant portion of the HuR surface, as can be

observed by following the movement of the center of mass of **6a** (Figure 9A-D), its RMSD vs time (Supporting Figure 3A) or its distance from the center of mass of the two RRM domains (Supporting Figure 3B). After about 1 μ s, each starting docking pose got stabilized and evolved to different final binding modes (Figure 9E-H) which remain individually stable for almost 500 ns. Specifically, out of the four final binding poses one was located outside the RNA binding cleft (the Glide predicted binding pose, Figure 9E) while the other three were located within the latter pocket, in correspondence or in close proximity of the “hinge” loop. In these final poses **6a** stabilizes HuR in a conformational state that is structurally incompatible with RNA binding. In fact, in each case the two RRM domains were found to be more in contact with each other than in the HuR-RNA complex crystal structure (Figure 9E-H). Accordingly, we observed an increase in both the number of non-native inter-domain contacts and the amount of surface area “buried” between the two RRM domains (see respectively Supporting Figure 4A and 4B). These results indicate that binding of **6a** to HuR is correlated with a closure of the RNA binding cleft and, consequently, with an overall decrease in the amount of inter-domain space accessible for RNA binding.

Nevertheless, among the four poses issuing from our modeling approach, the one depicted in Figure 10F and more in detail in Figure 11 seems to be more in agreement with both the NMR data and the SARs reported here. Specifically, **6a** was found between the RRM1 beta sheets (β 1, β 2, β 3), the N-terminal part of the RRM2 α 2 helix and the “hinge” loop. In this binding arrangement, (Figure 11) the phenyl ring in R_1 is accommodated in a narrow, laterally open, hydrophobic pocket, shaped by Ile103, Ser99, Lys104 and Lys156 residues, with which it establishes several CH- π interactions. Notably, one sulfonyloxygens establishes a water-bridged H-bond with the backbone C=O of Ala96, while the phenyl ring in R_2 , forms a cation- π interaction with Lys156 and several CH- π interactions with the CH₂ groups of Ser48, Lys50, Asn67 and Lys156. The indole-4,5-dione moiety is inserted in a solvent exposed pocket, where it

establishes CH- π interactions with Ala96, Lys156, Ser158 and, a π -stacking interaction with Phe65. In this regard, the quinone-oxygens, which point to the solvent exposed part of the pocket, likely play a crucial role in strengthening the π -stacking interaction with Phe65.

As compared to the other poses, in the above-described binding mode, **6a** is in close proximity with a larger number of HuR residues exhibiting the highest decreases in NMR signal intensity (Figure 8A). Precisely, these residues are Leu22, Val66, and Ile103. Noteworthy, NMR pinpointed Ile103 in the “hinge” loop as a residue sensitive to binding of **6a** but not of **1**, which is known to stabilize HuR in a closed form without stably interacting with the “hinge” loop³⁸. As compared to the other binding poses, which are located either outside the RNA binding cleft or in more solvent exposed regions, this binding mode (**Figure 11**) would be in line also with SARs studies. It would explain why substitutions on the phenyl ring in R₁ (**6f**, **6g**, **6h**, **6i**, **6k**, **6l**), though still causing a drop in the activity, are generally better tolerated than those on the phenyl ring in R₂ (**6b**, **6c**, **6d**, **6e**). In fact, thanks to the additional lateral space in the pocket hosting the phenyl ring in R₁, this ring could slightly rotate around the S-N bond so as to allow the attachment of various substituents, even large ones as in the case of **6k**. This would not be possible at position R₂, owing to potential steric clashes with residues shaping the pocket where it is hosted. This binding mode would also explain why the addition of electron-drawing substituents on the phenyl group in R₁ (**6f**, **6g**, **6h**, **6i**), particularly at the meta position (**6g**, **6i**), also causes a drop in the activity. In fact, these substitutions would likely weaken the aforementioned water-bridged H-bond with Arg97. Finally, SARs indicate that the addition of rigid and bulky substituents at position 6-7 (see **6w**) or 7 (**6p**, **6q**, **6r**, **6s**, **6t**) of the bicyclic scaffold (B ring) is also generally detrimental to binding. Steric clashes with the adjacent sulfonamidic group are very likely to arise as a result of their introduction, which would force a rotation around the S-N bond. That, according to our model, would in turn lead to a rupture of the water-bridged H-bond with Ala96 and of the hydrophobic interactions of the phenyl ring in R₁. In the case of **6q**, but especially of **6r** and **6s**, the presence of a H-bond donor at position 7 may partially

compensate for these detrimental effects through the potential formation of a H-bond with the near Arg⁹⁷ side chain. The only exception to this trend is represented by **6n**, where the presence of a sulfur atom directly linked to the scaffold likely increases the rotational flexibility and makes the addition of a bulky group well tolerated.

In conclusion, our NMR and molecular modeling data provide useful insights into the binding mode and mechanism of action of this family of compounds, suggesting that they most likely bind HuR at the “hinge” region between the two RRM domains and stabilize HuR in a peculiar closed conformation, which is incompatible with RNA binding.

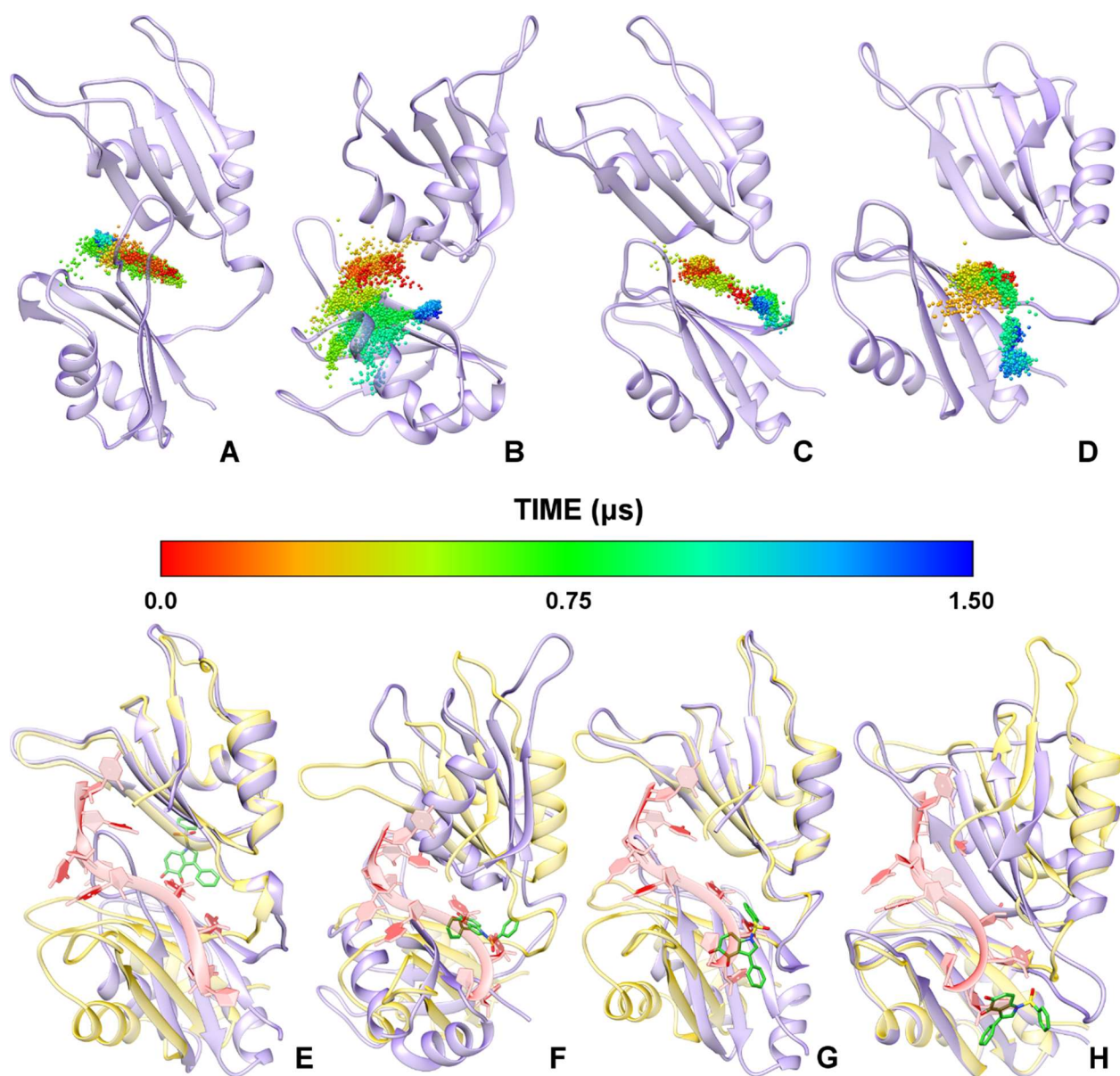


Figure 9.(A-D)**6a**exploration of the HuR RNA-binding pocket for each simulated pose. HuR is shown as purple cartoons, while the **6a** center of mass is shown as spheres colored according to the simulation time. (E-F) Global view of the HuR-**6a** complexes in each final MD simulation pose. Note how the binding of **6a** (green sticks) to HuR and the further closure of the mRNA binding cleft, as compared to the mRNA-bound conformation (yellow), prevent the accommodation of the mRNA strand

(red ribbons). In both groups of pictures, panels related to the pose predicted by Glide and the three highest score poses predicted by Autodock are arranged from left to right, respectively.

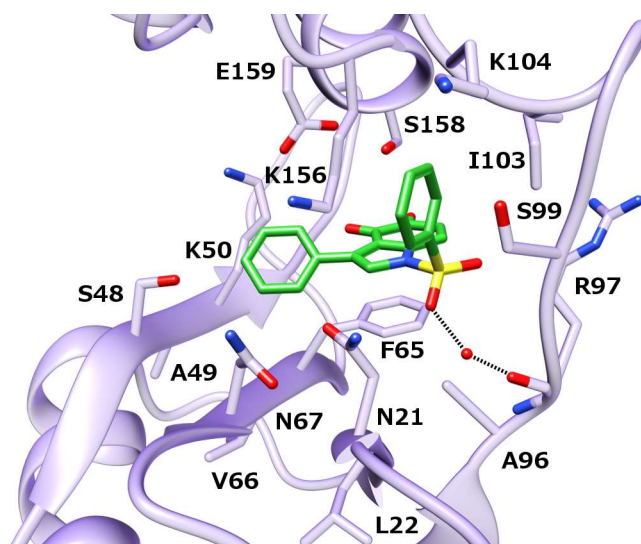


Figure 10. Most likely binding mode of **6a** (green sticks) to HuR (purple cartoons), as issuing from a representative structure of the last 500ns of the MD simulation. HuR residues involved in binding interactions with **6a** are displayed as sticks.

Biological activity in cancer cell lines

Selected aza-tanshinones show micromolar cytotoxicity in cancer cells. We previously reported that the anti-cancer effects of DHTS are influenced by HuR dosage, demonstrating that HuR is functionally connected with the intracellular effects of this pleiotropic natural product³⁸. Similarly to DHTS, the localization of HuR did not change during treatment with **6a** or other aza-tanshinones,

suggesting that inhibition of HuR is connected with its binding performances and not with its subcellular localization (Figure 11).

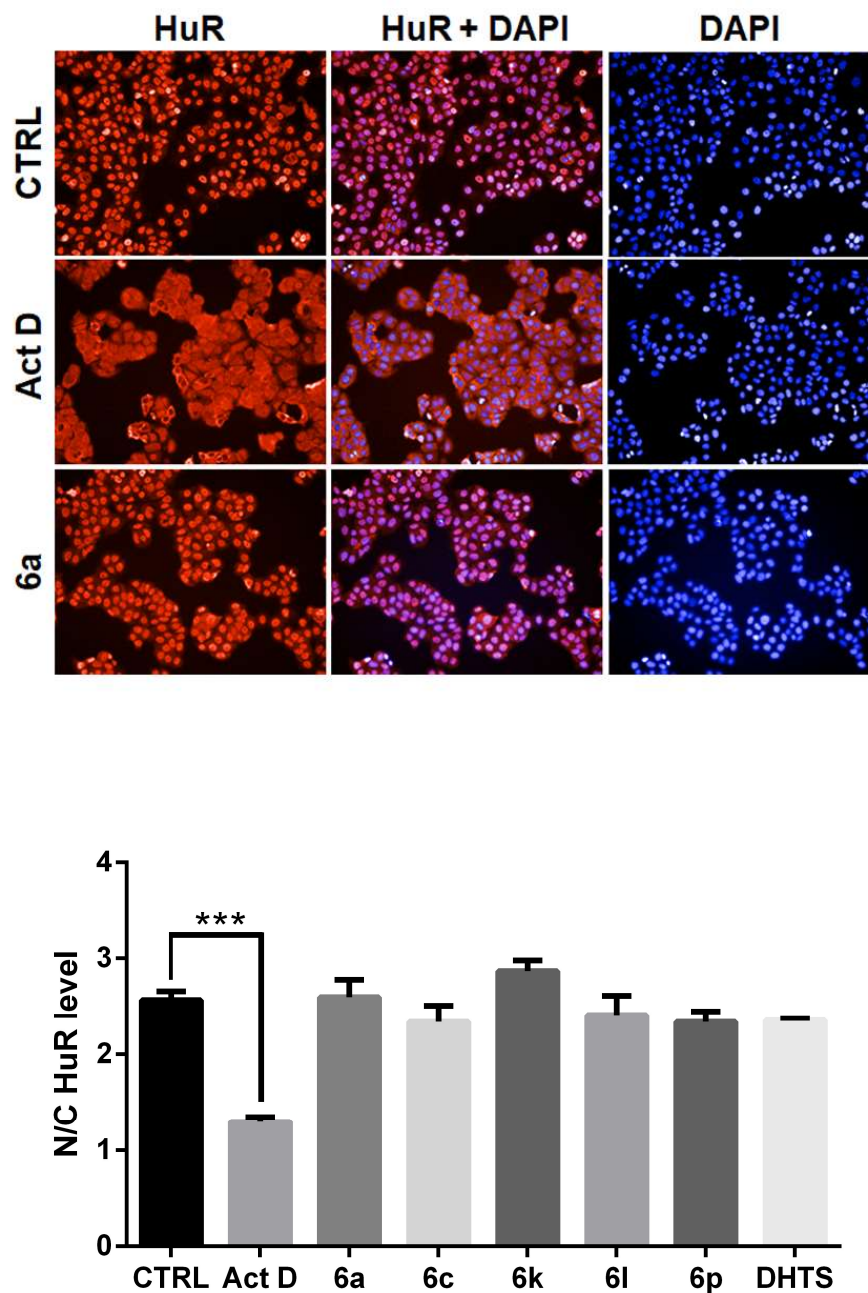
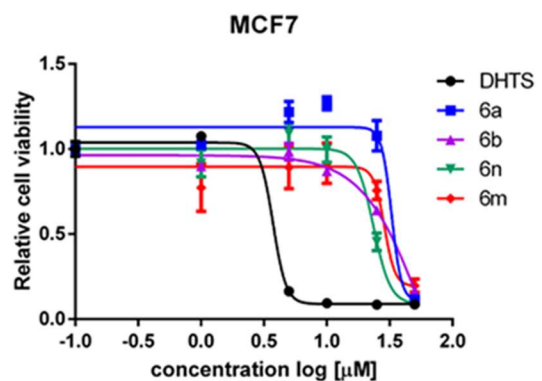


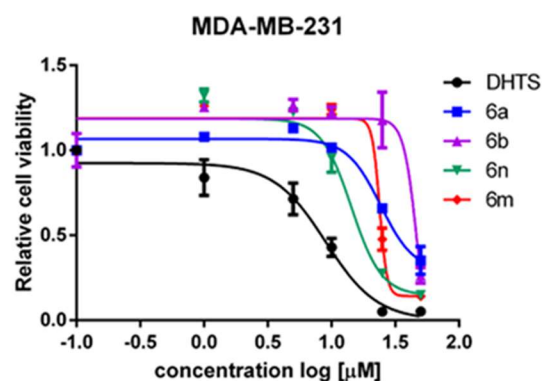
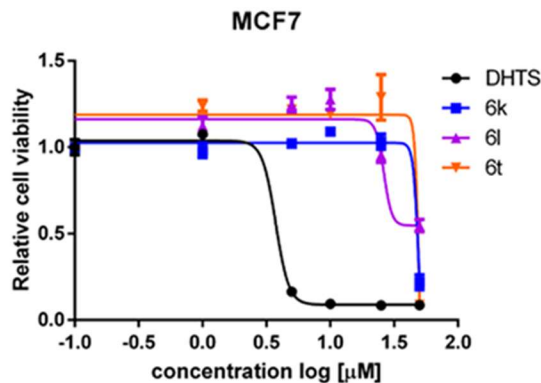
Figure 11. Representative immunofluorescence showing unchanged subcellular localization of HuR after **6a** treatment. HuR (red) or nuclei (blue DAPI) after staining in MCF-7 cells treated for 3 h with DMSO (CTRL) or 2.5 μ M of Actinomycin D (ActD) or 10 μ M **6a**. Plotted in the graph are the ratio

of HuR fluorescent signal between nucleus and cytoplasm (N/C). The image plate reader Operetta was used for image acquisition and evaluation by selecting 13 fields/well. The ratio N/C represents the mean \pm SD of single cells for every well (**p<0.001).

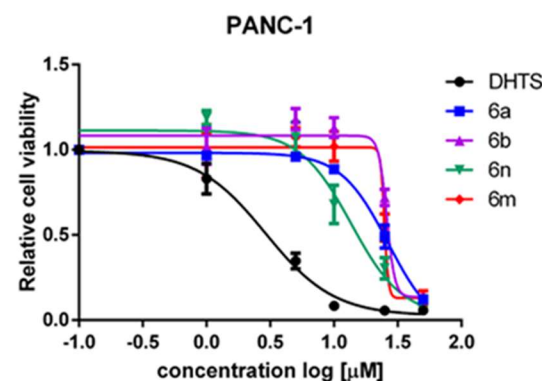
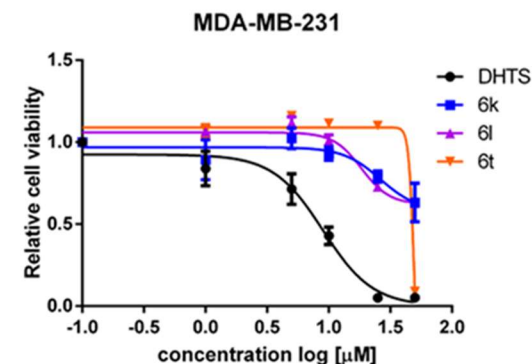
We evaluated the cytotoxic effects of aza-tanshinones. Compounds **6a** and **6n** affected the viability of cells when treated for 72 hrs, together with **6b**, **6m**, **6k**, **6l** and **6t** at higher dosages (Figure 12). They were tested on breast cancer cell lines MCF7 and MDA MB231, and on pancreatic ductal adenocarcinoma cell line PANC-1. Aza-tanshinones were generally less effective than DHTS on cell viability (Figure 12, Supporting Table 1), with an EC₅₀ in the medium μ M range (spanning from 20 to 50 μ M for compounds **6a**, **6b**, **6n** and **6m**, Figure 12, PANC-1 being the more sensitive cell line to the tested compounds). An IC₅₀ value was achieved for **6a**, **6b**, **6n**, **6m** compounds (Figure 12).



	DHTS	6a	6b	6n	6m
IC ₅₀	~ 3.73	~ 32.69	58.52	23.49	~ 28.67
R ²	0.9957	0.9280	0.9797	0.9649	0.8621



	DHTS	6a	6b	6n	6m
IC ₅₀	8.99	24.17	~ 47.18	14.31	~ 23.79
R ²	0.9643	0.9680	0.9041	0.9432	0.9499



	DHTS	6a	6b	6n	6m
IC ₅₀	2.91	26.47	~ 25.90	13.62	~ 24.88
R ²	0.9861	0.9915	0.9528	0.9531	0.9589

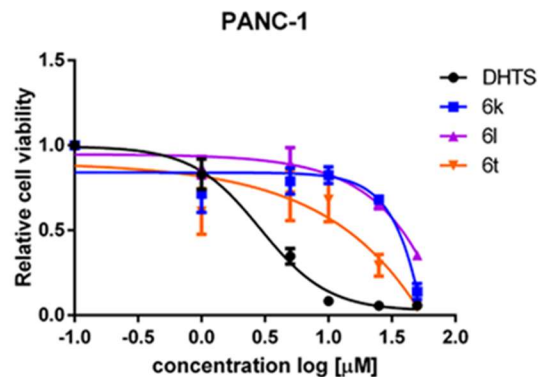
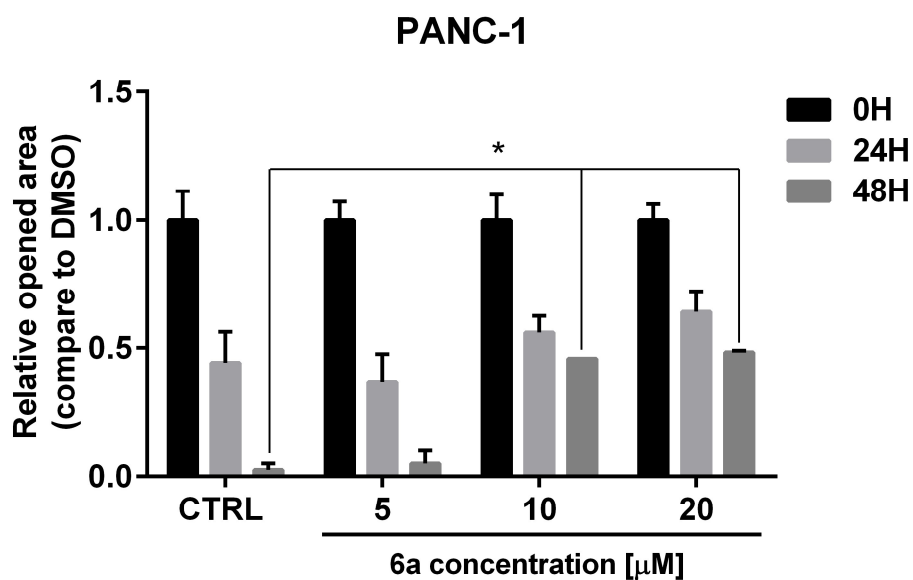


Figure 12. Cell viability of aza-tanshinones, assessed after 72 h of treatment with the indicated compounds (0-50 μ M). Plotted bars are mean \pm SD of a biological duplicate, normalized to control (DMSO). Relative IC₅₀ and R2 were calculated by nonlinear regression curve fitting.

Additionally, aza-tanshinone**6a** could block the migration of PANC1 and MDA MB231 cells (Figure 13A, B and Supporting Figure 5). Therefore, aza-tanshinones do not affect HuR mobility directly and are endowed with interesting anti-tumor properties.



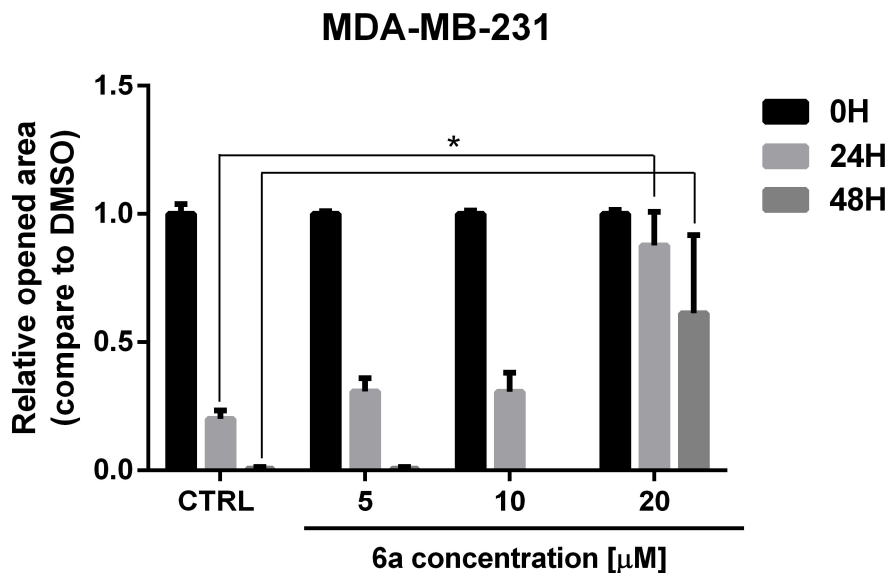


Figure 13. Scratch assay in PANC-1 and MDA-MB-231 cells. Images of invaded cells at 0, 24, and 48 h after scratching and treatment with control (DMSO) or **6a** were taken from a time-lapse sequence of cell migration; wounds with consistent shape within each well were generated using 200 μ l tip. Residual open area at different time points is indicated as calculated by ImageJ software (* $p < 0.05$).

CONCLUSION

In our previous effort, as a result of a high throughput screening on a set of anti-inflammatory agents, we identified Dihydratanshinone-I (**1**, DHTS), a low molecular weight compound able to interact with HuR, thus affecting its post-transcriptional functions and contributing to its cytotoxic properties²⁴. Very recently, we characterized its mechanism of action through a multi-disciplinary strategy³⁸. Here, inspired by DHTS structure, we designed and synthesized an array of orto-quinones (aza-tanshinones). They are the first family of HuR disruptors, through which the SAR reported here elucidates the steric/electrostatic requirements of an HuR binding site. To this regard, two complementary techniques, Alpha-Screen and REMSA, were used to quantify the inhibitory activity of aza-tanshinones **6a-t**. Among them, compounds **6a** and **6n** turned out to be more effective than DHTS in HuR binding, showing a Ki

of 12.8 and 15 nM respectively. In addition, **6a** is the only molecule, to our knowledge, for which a direct K_d against HuR can be measured through DMR (K_d ≈ 4.5 μM). A combined approach of *in vitro* studies, NMR titration and Molecular Dynamic simulations clarified the mechanism of action of compound **6a**. Namely, **6a** most likely binds HuR at the “hinge” region between the two RRM domains, in accordance with the docking-based analysis of different HuR-mRNA disruptors⁴². Docking did not reveal the most likely pose that **6a** assumes when interacting with HuR, that could only be achieved by a complementary MD-NMR approach, due to the high flexibility of the protein. Although DHTS and **6a** have been predicted to bind different sub-pockets of the same binding region³⁸, specifically at the interface between the two RRM domains, they seem to share a common mechanism of action, that is to stabilize HuR in a peculiar closed conformation, which is incompatible with RNA binding.

From a biological point of view, previously identified HuR disruptors show cytotoxic activity in cancer cell lines and in xenograft models. MS-444 inhibited viability and migration of breast cancer cell lines and induced cell death in colon cancer cells xenografted in nude mice⁴³, and as did coumarin analogs in colon cancer cells *in vitro*⁴⁴. Additionally, MS-444 chemo-prevented the development of intestinal tumors in APC^{min} mice, a model of familial adenoma familial adenomatosis polyposis, but was detrimental in the context of chemically induced inflammatory bowel disease (IBD)⁴⁵. In this case, MS-444 favored azoxymethane/ dextran sodium sulphate AOM/DSS tumorigenesis, size and invasiveness, therefore suggesting a careful evaluation of the utilization of HuR disruptors in the IBD settings.

1 (DHTS) inhibited viability and migration of breast cancer cell lines and induced cell death in colon cancer cells xenografted in nude mice in a HuR dependent manner³⁸, although its pleiotropic effects contribute to its activity. Aza-tanshinones **6a**, **6b**, **6m**, **6n**, **6k**, **6l** and **6t** showed moderate IC₅₀ in cancer cell lines, that was comparable to MS-444 (5 to 15 μM in colon cancer cell lines)⁴³ and coumarin analogs (50 to 75 μM effective doses colon cancer cell lines)⁴⁶. The diminished cytotoxicity of aza-tanshinones

compared to DHTS could be ascribed to the reported multi-pharmacological effects of the latter⁴⁷, or to limited bioavailability of aza-tanshinones. Nevertheless, our first generation aza-tanshinones are a valuable starting point to generate a more potent, *in vivo* active set of anticancer compounds. Our current efforts aim to further expanding our SAR, and to improve the efficacy of aza-tanshinones on HuR modulation in cells through the introduction of solubilizing moieties in position 1 and 7.

EXPERIMENTAL SECTION

Chemistry

General Procedures. ¹H NMR spectra were recorded on a Bruker Avance 400MHz instrument in CDCl₃, CD₃OD or D₂O as solvent at 400 MHz. ¹³C NMR spectra were recorded in CDCl₃, CD₃OD or D₂O as solvent at 101 MHz. Coupling constants are given in Hertz and are rounded to the nearest 0.1 Hz. LC–MS data were collected with a Waters AcquityTM Ultra performance LC equipped with an Acquity UPLCTM HSS T3 column (2.1 mm x 50 mm, 1.8 μm) and a SQD detector. Purifications were carried out either by flash chromatography on silica gel (particle size 60 μm, 230–400 mesh), on Kieselgel, or by BiotageTM flash chromatography [Biotage columns Si-25-M (150 x 25 mm; silica gel (40–63 μm), flow rate 25 mL/min)], or by BiotageTM C₁₈ reverse phase chromatography [Biotage column C₁₈HS (150 x 25 mm; KP-C₁₈-HS (35–70 μm), flow rate 25mL/min)]. Final compounds **6a-i**, **6k-p**, **6s** were purified by C₁₈ reverse phase semi-preparative HPLC using a Waters X-Bridge column (19 mm x 15.0 cm, 5 μm). Solvents were distilled and dried according to standard procedures, and reactions requiring anhydrous conditions were performed under nitrogen or argon atmosphere.

3-bromo-5-methoxyindole (8). The synthesis of compound **8** was carried out as previously described [43], and its analytical characterization confirmed its structure.

1-Phenylsulfonyl-3-bromo-5-methoxyindole (11). The synthesis of compound **11** was carried out as previously described⁴⁸, and its analytical characterization confirmed its structure.

1-Phenylsulfonyl-3-phenyl-5-methoxyindole (9a). The synthesis of compound **9a** was carried out as previously described⁴⁹, and its analytical characterization confirmed its structure.

1-Phenylsulfonyl-3-phenyl-5-hydroxyindole (12a). 1M BBr₃ in CH₂Cl₂ (26.4 mL, 6 eq) was slowly added under nitrogen atmosphere and at -78 °C to a stirred solution of 1-phenylsulfonyl-3-phenyl-5-methoxy indole **9a** (1.6 g, 4.41 mmol, 1 eq) in dry CH₂Cl₂ (22 mL, ≈0.2 M concentration). The temperature was slowly raised to room temperature while monitoring by TLC (eluants: n-Hexane/EtOAc 8/2). The resulting dark green solution was immediately diluted with water (150 mL) and neutralized with saturated aqueous NaHCO₃. The reaction mixture was extracted with CH₂Cl₂ (3 x 150 mL). The collected organic phases were then washed with brine (400 mL), dried over Na₂SO₄, and filtered. The solvent was removed under reduced pressure. The crude (1.7 g) was purified by flash chromatography on silica gel, yielding pure compound **12a** (1.34 g, 3.84 mmol, **87%** yield) as a white solid. **¹H_NMR (400 MHz, acetone d₆):** δ(ppm) 8.29 (s, 1H, OH), 8.05-8.03 (m, 2H, o-ArSO₂), 7.93 (d, 1H, J = 8.9 Hz, H7), 7.84 (s, 1H, H2), 7.69-7.65 (m, 3H, p-ArSO₂, o-Ar), 7.60-7.56 (m, 2H, m-ArSO₂), 7.50-7.46 (m, 2H, m-Ar), 7.38 (tt, 1H, J = 7.4 Hz, J = 1.2 Hz, p-Ar), 7.21 (d, 1H, J = 2.4 Hz, H4), 6.96 (dd, 1H, J = 8.9 Hz, J = 2.4 Hz, H6). **¹³C_NMR (75.4 MHz, acetone d₆):** δ(ppm) 155.5, 138.9, 135.1, 134.0, 131.4, 130.4, 129.8, 128.6, 128.4, 127.8, 124.9, 115.6, 115.0, 106.0. **MS (ESI⁺):** m/z 721.0 [2M+Na⁺]. Calculated MS, C₂₀H₁₅NO₃S: 349.08.

1-Phenylsulfonyl-3-phenyl-4,5-dioxindole (6a). IBX [28] (548 mg, 1.96 mmol, 1.2 eq) was added to a solution of 1-phenylsulfonyl-3-phenyl-5-hydroxy indole **12a** (570 mg, 1.63 mmol, 1 eq) in EtOAc (8 mL, ≈0.17M concentration), under vigorous stirring at room temperature. The reaction was monitored by TLC (eluants: n-Hexane/EtOAc 6/4). After 24 hours the reaction was filtered on celite.

After concentration of the solvent, the crude (930 mg, purple solid) was purified by flash chromatography on silicagel (eluants: n-Hexane/EtOAc 6/4). Pure compound **6a** (515 mg, 1.42 mmol, **87%** yield) was obtained as a dark red solid. **¹H_NMR (400 MHz, acetone d6):** δ (ppm) 8.25-8.23 (m, 2H, **o**-ArSO₂), 8.07 (d, 1H, J = 10.5 Hz, H7), 7.87 (tt, 1H, J = 7.5 Hz, J = 1.2 Hz, **p**-ArSO₂), 7.78-7.74 (m, 3H, H2, **m**-ArSO₂), 7.68-7.65 (m, 2H, **o**-Ar), 7.40-7.33 (m, 3H, **p**-Ar, **m**-Ar), 6.21 (d, 1H, J = 10.5 Hz, H6). **¹³C_NMR (75.4 MHz, acetone d6):** δ (ppm) 182.3, 174.8, 138.5, 137.9, 136.5, 132.1, 131.5, 131.3, 130.5, 129.6, 129.1, 128.9, 128.5, 127.1. **MS (ESI⁺):** m/z 748.9 [2M+Na⁺]. Calculated MS, C₂₀H₁₃NO₄S: 363.06.

3-Phenyl-5-methoxyindole (14). Aqueous 3M NaOH (21 mL, 63 mmol, 46 eq) was added dropwise in 30 minutes to a solution of 1-phenylsulfonyl-3-phenyl-5-methoxy indole **9a** (500 mg, 1.38 mmol, 1 eq) in 2/1 MeOH/THF (207 mL). The pale pink mixture was warmed up to 80°C. The reaction was monitored by TLC (eluant: n-Hex/EtOAc 8/2). After 2 hours the reaction was stopped by acidifying with 3N HCl (21 mL), and the organic solvents were evaporated under reduced pressure. The aqueous residue was extracted with EtOAc (3 x 100mL). The collected organic layers were washed with brine (450 mL), and dried over sodium sulfate. The solvent was evaporated under reduced pressure affording a crude brown oil (365 mg), that was purified by flash chromatography on silica gel (eluant: n-Hex/EtOAc 85/15). Pure compound **14** (300 mg, 1.34 mmol, **97%** yield) was obtained as a pale yellow solid. **¹H_NMR (400 MHz, acetone d6):** δ (ppm) 10.33 (1H, bs, NH), 7.72-7.69 (2H, m, **o**-Ar), 7.58 (1H, d, J = 2.6 Hz, H2), 7.47-7.36 (4H, m, H4, H7, **m**-Ar), 7.26-7.21 (1H, m, **p**-Ar), 6.85 (1H, dd, J = 2.50 Hz, J = 8.80 Hz, H6), 3.84 (3H, s, OMe). **MS (ESI⁺):** m/z 748.9 [2M+Na⁺]. Calculated MS, C₁₅H₁₃NO: 223.27.

1-Phenylsulfonyl-3-aryl-5-substituted indoles, general Suzuki procedure (9b,c, 12d,e). 1-Phenylsulfonyl-3-bromo-5-methoxy- (**11**) or 5-hydroxy indole (**13**) (1 eq) and an arylboronic acid (1.17

eq) were placed in a two-necked round-bottom flask, equipped with a CaCl_2 valve. The flask was flushed with nitrogen to remove any trace of oxygen. The middle neck was closed by a rubber septum, then dry dimethoxyethane (DME, $\approx 0.07\text{M}$ concentration in **11**) and previously deaerated aqueous 2M K_2CO_3 (1.29 eq) were added and the resulting mixture was stirred at rt under nitrogen atmosphere. Finally, PdTetrakis (0.05 eq) and previously deaerated EtOH (final 4/1 DME/EtOH ratio) were added under nitrogen flushing. A pale yellow solution was formed. The rubber septum was removed, then the main-middle neck was equipped with a condenser surmounted by a CaCl_2 valve. The pale yellow solution was stirred under nitrogen atmosphere, refluxed for 8 hours and left stirring at room temperature overnight. Then, the reaction mixture was diluted with a saturated solution of NH_4Cl (one volume) and extracted with EtOAc (1.5 volumes, three times). The organic phase were washed with saturated aqueous NH_4Cl (three volumes) and with brine (three volumes), then dried over Na_2SO_4 and filtered. The crude was purified by flash chromatography on silicagel,affording pure 1-phenylsulfonyl-3-aryl-5-substituted indoles as amorphous solids.

1-Arylsulfonyl-3-phenyl-5-methoxyindoles, general N-arylsulfonylation procedure (9f-i). Aqueous 50% KOH (8 eq) was added to a stirred mixture of 3-phenyl-5-methoxy indole **14** (1 eq) and $n\text{-Bu}_4\text{N}^+\text{HSO}_4^-$ (0.1 eq) in CH_2Cl_2 ($\approx 0.2\text{M}$ concentration in **14**). The reaction was stirred vigorously at room temperature for 10 minutes. An arylsulfonylchloride (1.7 eq) in CH_2Cl_2 (total $\approx 0.1\text{M}$ concentration in **14**) was then added, and the mixture turned to orange-brown. The reaction was monitored by TLC (eluant: n-Hex/EtOAc 9/1). After 3 hours the reaction was stopped by diluting with water (one volume) and extracting with CH_2Cl_2 (two volumes, two times). The collected organic layers were washed with water (two volumes) and brine (two volumes), and dried over sodium sulfate. The solvent was evaporated under reduced pressure affording a crude. The crude was purified through flash chromatography on silicagel,affording pure 1-arylsulfonyl-3-phenyl-5-methoxy indoles as amorphous solids.

1-Aryl/alkylsulfonyl-3-substituted-5-hydroxyindoles, general demethylation procedure (12a-c, 12f-i, 12k, 12l, 13). 1M BBr₃ in CH₂Cl₂ (6 eq) was slowly added under nitrogen atmosphere and at -78 °C to a stirred solution of 1-aryl/alkylsulfonyl-3-substituted-5-methoxy indoles (1 eq) in dry CH₂Cl₂ (≈0.2 M concentration). The temperature was slowly raised to room temperature while monitoring by TLC, then it was immediately diluted with water (five volumes) and neutralized with saturated aqueous NaHCO₃. The reaction mixture was extracted with CH₂Cl₂ (five volumes, 3 times). The collected organic phases were then washed with brine (fifteen volumes), dried over Na₂SO₄, and filtered. The solvent was removed under reduced pressure. The crude hydroxyl indoles were purified by flash chromatography on silicagel, affording pure 1-aryl/alkylsulfonyl-3-substituted-5-hydroxy indoles as amorphous solids.

1-Alkyl/arylsulfonyl-3-phenyl-4,5-dioxoindoles, general oxidation procedure A (6a, 6f-h, 6l). IBX [28] (1.2 eq) was added to a solution of 5-hydroxy indoles (1 eq) in EtOAc (≈0.17M concentration), under vigorous stirring at room temperature. The reaction was monitored by TLC. When the reaction was completed (between 7 and 34 hours), the mixture was filtered on celite. After concentration of the solvent, the crude was purified by flash chromatography on silicagel, affording pure 1-arylsulfonyl-3-aryl-4,5-dioxo indoles as amorphous solids.

1-Arylsulfonyl-3-aryl-4,5-dioxoindoles, general oxidation procedure B (6b-e, 6i, 6k). IBX [28] (1.2 eq) was added to a solution of 5-hydroxy indoles (1 eq) in DMF (≈0.17M concentration), at room temperature and under vigorous stirring. The reaction was monitored by TLC. When the reaction was completed (between 2 and 48 hours), the mixture was diluted with water (20 volumes). The aqueous phase was extracted with EtOAc (10 volumes, until colorless). The collected organic layers were washed once with brine (20 volumes), dried with anhydrous Na₂SO₄ and filtered. The solvent was removed under

reduced pressure, and the resulting crude was purified by flash chromatography on silicagel,affording pure 1-arylsulfonyl-3-aryl-4,5-dioxo indoles as amorphous solids.

1-Phenylsulfonyl-3-phenyl-7-thioaryl-4,5-dioxoindoles, general procedure for Michael reaction (6m-o).

A substituted thiophenol (1.18 eq) was added to a solution of 1-(phenylsulfonyl)-3-phenyl-4,5-dioxo indole **6a** (1.0 eq) in DMF (0.23M). The solution was stirred at rt for 2-3 hours, then water (one volume) was added. The mixture was extracted with EtOAc (4 x four volumes), the collected organic phases were dried over sodium sulfate, filtered and evaporated under reduced pressure. The crude was purified by reverse phase chromatography (eluants: A CH₃CN, B water, from 0% A to 100% A), affording the orto-bisphenol (62%-88%).

IBX (0.5-2 eq) was then added to the orto-bisphenol (1eq) in DMF (0.2 M) under stirring at rt. After reaction completion (2 hours), water was added (1 volume) and the mixture was extracted with EtOAc (4 x 2 volumes). The collected organic phases were dried over sodium sulfate, filtered and evaporated under reduced pressure. The crude residue was purified by reverse phase chromatography (eluants: A CH₃CN, B H₂O, from 0% A to 100% A) affording pure 1-(phenylsulfonyl)-3-phenyl-7-thioaryl-4,5-dioxo indoles as amorphous solids.

1-Phenylsulfonyl-3-phenyl-7-thiophenyl-4,5-dioxoindole (6m). The title compound (30.2 mg, 45% yield over 2 steps, purple solid) was prepared from 1-(phenylsulfonyl)-3-phenyl-4,5-dioxo indole **6a** (55 mg, 0.15 mmol, 1.0 eq) and thiophenol (18.2 μ l, 0.178 mmol, 1.18 eq) in DMF (0.65 mL), following the general procedure for Michael reaction (2.5 hrs) and IBX oxidation. **¹H_NMR (400 MHz, acetone-d₆):** δ (ppm) 7.89-7.63 (m, 12H, Ar), 7.59 (s, 1H, H₂), 7.42-7.31 (m, 3H, Ar), 6.91 (s, 1H, H₆). **¹³C_NMR (100 MHz, acetone-d₆):** δ (ppm) 177.2, 173.6, 140.3, 138.1, 137.2, 135.7, 135.6, 131.2, 130.5, 130.4,

129.1, 129.0, 128.5, 128.1, 128.0, 127.3, 122.3, 120.9, 119.5. **MS (ESI⁺):** *m/z* 494.32 [M+Na⁺].

Calculated MS, C₂₆H₁₇NO₄S₂: 471.06.

1-Phenylsulfonyl-3-phenyl-7-alkyl/aryl-4,5-dioxoindoles, general procedure for Mn(III)-mediated radical addition (6p-t). 1-(phenylsulfonyl)-3-phenyl-4,5-dioxo indole **6a** (1.0 eq) and a boronic acid (1.5 eq) were dissolved in dry dichloroethane (DCE, ≈0.09 M in **6a**). The solution was stirred for 2 minutes and then Mn(OAc)₃·2H₂O (3 eq) was added. The mixture was kept under nitrogen atmosphere, stirred at 80°C until reaction completion (monitoring by TLC, eluants: n-Hexane/EtOAc 7/3), and cooled at room temperature. Then, CH₂Cl₂ (2 volumes) and saturated aqueous NaHCO₃ (2 volumes) were added. The aqueous layer was extracted with CH₂Cl₂ (2 volumes x 4 times). The collected organic phases were washed with brine (8 volumes x 2 times), dried over sodium sulfate, filtered and evaporated under reduced pressure to give a crude solid. The crude was purified by flash chromatography (eluants: n-Hexane/EtOAc 7/3). Pure 1-(phenylsulfonyl)-3-phenyl-7-substituted-4,5-dioxo indoles were obtained as amorphous solids.

1-Phenylsulfonyl-3,7-diphenyl-4,5-dioxoindole (6p). The title compound (32 mg, 0.072 mmol, purple solid, **34%** yield considering the recovery of 28 mg of unreacted **6a**) was obtained from 1-(phenylsulfonyl)-3-phenyl-4,5-dioxo indole **6a** (105 mg, 0.289 mmol, 1.0 eq) and phenylboronic acid (55 mg, 0.452 mmol, 1.5 eq) in dry DCE (3 mL, ≈0.09 M), following the general procedure for Mn(III)-mediated radical addition. **¹H_NMR (400 MHz, DMSO d₆):** δ(ppm) 8.27 (2H, d, J = 7.7 Hz, o-Hs of PhSO₂), 7.96 (1H, s, H₂), 7.89-7.83 (2H, m, H₆, p-H of PhSO₂), 7.76 (2H, t, J = 7.7 Hz, m-Hs of PhSO₂), 7.72-7.76 (2H, m, o-Hs of 3-Ph), 7.50-7.36 (8H, m, m- and p-Hs of 3-Ph, all Hs of 7-Ph). **¹³C_NMR (75.4 MHz, DMSO d₆):** δ(ppm) 179.5, 173.4, 137.0, 136.8, 136.0, 134.9, 130.9, 130.6, 128.7, 128.3, 128.1, 127.6, 125.0, 123.8, 121.3. **MS (ESI⁺):** *m/z* 440.21 [M+H⁺]. Calculated MS, C₂₆H₁₇NO₄S: 439.09.

Biology

Amplified Luminescent Proximity Homogeneous Assay (ALPHA Screen). AlphaScreen assays have been performed using histidine (nickel) chelate detection kit (Perkin Elmer, 6760619), based on the reaction of an His-tagged HuR protein and a biotinylated single strand RNA (BITEG-RNA), as previously described³⁴. The full-length human recombinant protein has been expressed in *E.coli* Rosetta DH5 α according to an already published protocol²⁴. Hooking point curves, with 50 nM of BITEG-RNA probe, have been performed to test its activity after purification and dialysis. Dissociation equilibrium constants (K_i) were calculated with respect to a K_d of 2.5 nM for the Bi-AU ligand interaction, in the presence of as low as 0.5% DMSO (relative control) and of aza-tanshinones. Nonspecific interference with the assay has been evaluated by reacting the same amount of Acceptor and Donor beads (20 μ g/ml/well) with biotinylated-His₆ molecule in the same experimental conditions. Dissociation experiments were performed upon 30 min pre-incubation of 1 nM of rHuR and 50 nM of RNA plus beads before addition of DHTS or **6a**, as previously described²⁴. GraphPad Prism software v5.1 has been used for fitting calculation and statistical significance.

RNA-Electrophoretic mobility shift assays (REMSAs). REMSAs were performed as previously indicated²⁴, with minor modifications. At least 10 fold excess of recombinant HuR was incubated for 30 min with either 50 fmol of 5'-DY681-labeled AU-rich RNA probe or with 25 nM of 5'-FAM-labeled RNA probe and DMSO as control or aza-tanshinones (5 μ M), then loaded on 4% native polyacrylamide gel. The gel image was developed with Odyssey infrared Imaging System (LI-COR Biosciences) for DY681-labeled RNA or in Typhoon Trio scanner (GE Healthcare) at high resolution for FAM probe at 488nm.

Dynamic Mass Redistribution (DMR). The EnSight Multimode Plate Reader (Perkin Elmer) was used to perform DMR analyses. Full length HuR protein (15 μ L/well of a 50 μ g/ml HuR solution in 20 mM sodium acetate buffer, pH 5.5) was immobilized on label-free microplate (EnSpire-LFB high sensitivity microplates) by amine-coupling chemistry, incubating the microplate o/n at 4°C. After equilibrating the plate with the assay buffer (HEPES 25 mM pH 8, 3 mM $MgCl_2$, 100 mM NaCl, 8% Glycerol, 0.05% BSA, 0.005% Tween20), the interaction between aza-tanshinones, diluted to different concentrations in the same buffer, and HuR protein was monitored during 30 min at room temperature. All the steps were executed by employing a Zephyr Compact Liquid Handling Workstation. The Kaleido software was used to acquire and process the data.

Cell culture. Human breast adenocarcinoma MCF7 (ICLC; HTL95021) and MDA-MB-231 (ICLC; HTL99004) and pancreatic carcinoma PANC-1 (kindly provided by G. Feldmann, ⁵⁰) cell lines were cultured in high glucose Dulbecco's modified Eagle's medium (DMEM) supplemented with 10 % fetal bovine serum (FBS, Lonza), 2 mM L-glutamine, 100 U/ml penicillin-streptomycin (Lonza) in standard growth conditions.

RNA immunoprecipitation (RIP) and quantitative real-time PCR (qRT-PCR). Five millions MCF7 cells/sample were used for each RIP experiment, performed as previously described ⁵¹, without cross-linking steps and using 1 μ g/ml of anti-HuR antibody (Santa Cruz, 71290) or of mouse IgG isotype (negative control, Santa Cruz 2025). TRIzol reagent was added directly to the beads for HuR-bound RNA isolation and processed for qRT-PCR analysis. Quantitative PCRs, after cDNA Synthesis (Thermo Scientific, K1612) were performed using Universal SYBR Master Mix (KAPA Biosystems, KR0389) on CFX-96/384 thermal cyclers (BIO-RAD), as previously described ²⁴. Fold enrichment was determined using the equation $2^{-\Delta\Delta C_t}$, where the C_t value for INPUT, HuR and IgG IP was subtracted from the C_t

value of the housekeeping gene RPLP0 to yield the ΔC_t value. For each condition, the ΔC_t value for the HuR and IgG IP were computed in triplicate and averaged to the value obtained from the input sample. Total expression level of the different mRNAs was assessed by extracting total RNA from the control and treated samples and then qRT-PCRs have been performed as described previously. The sequence of the primer used for each PCR are the following: *RPLP0* (CATTCTCGCTTCCTGGAG and CTTGACCTTTTCAGCAAGTGG), *ERBB2* (GGTACTGAAAGCCTTAGGGAAGC and ACACCATTGCTGTTTCCTTCCTC), *VEGFA* (CCGCAGACGTGTAAATGTTTCCT and CGGCTTGTCACATCTGCAAGTA), *CTNNB1* (GACCTCATGGATGGGCTGCCT and GATTACAAATAGCCTAAACCAC).

Immunofluorescence experiments. 8.000 MCF7 cells/well were seeded in a 96-well plate and treated with 1 μ M of DHTS, or 10 μ M of aza-tanshinones, or 2.5 μ M of Actinomycin D (ActD, Sigma A1410) for 3 hrs and were fixed with 3.7% paraformaldehyde (PFA) for 15 min at RT. Cells were treated for 10 min with permeabilization buffer (200 mM sucrose, 0.2% Triton X-100) followed by blocking for 15 min with blocking buffer (2% Bovine Serum Albumin in PBS). Primary antibody anti-HuR 1:250 in 3% BSA and secondary fluorophore conjugated (Alexa 594 Red) antibody (1:500) were diluted in PBS + BSA 0.6%. DAPI Blue (1.5 μ g/ml) in PBS + BSA 0.6% was used to detect nuclei. PerkinElmer image plate reader Operetta was used for image acquisition and evaluation by selecting 13 fields/well. The ratio between nuclear and cytoplasmic signal represents the mean of single cells for every well.

Cell viability assay. To test cell viability, cells were grown and treated in 96 well-plate for 48 h. Cells were then assayed using OZBlue Cell Viability kit (Oz Biosciences, BL000). In brief, OZBlue was added at 10% volume of culture media to each well and cells were further incubated for 3 h at 37 °C. Fluorescence was then determined (excitation 560 and emission 590 nm) by Tecan microplate reader.

Cell survival was calculated with respect to control (DMSO) and IC₅₀ values were determined by fitting with GraphPad Prism software v5.1.

Cell migration assay. Cells were seeded for migration assay and treated with aza-tanshinones as previously described⁵². Images of the same field were acquired immediately (t = 0), after 24 and 48 hours using a Leica DM IL Led microscope (5X magnification) and wounded-open areas were measured using Image-J software.

Statistical analysis. All data are expressed as means \pm SD from at least two independent experiments. Magnitude of significance was evaluated by student t-test and probability (P) values <0.05, <0.01, and <0.001 were indicated with *, **, *** symbols, respectively.

NMR and MD studies

NMR measurements on protein/compound 6a interaction. The assignment of RRM1-RRM2 tandem domains of HuR was previously reported (BMRB code: 27002)⁵³. The effect of the aza-tanshinone **6a** on the RRM1-RRM2 tandem domains of HuR (100 μ M) has been evaluated in the following experimental conditions: 20 mM Tris-Cl, pH 8, 10 mM Gly, 50 mM NaCl. 2D ¹H ¹⁵N HSQC spectra were acquired at 298 K on Bruker Avance 900 MHz NMR spectrometer to monitor the effect of increasing amounts of the ligand (HuR/compound **6a** molar ratio of 1:0.2, 1:0.4, 1:0.6, 1:0.8, 1:1, 1:2) added to the protein solution.

Docking calculations. Molecular docking was carried out using the Glide 6.5⁵⁴ and the AutoDock 4.2⁵⁵ softwares. **6a** three-dimensional structure was first generated and subsequently prepared

through the LigPrep module, as implemented in the Maestro 10.0.013 graphical user interface⁵⁶. As experimental results suggest that I) HuR cannot bind both **6a** and RNA at the same time and that II) **6a** stabilizes HuR in a “closed” conformation, we selected as receptor structure for docking calculations the structure of the HuR-mRNA complex (PDB code: 4ED5)⁴⁰, and removed the RNA strand. Indeed this structure was not only the HuR highest resolution structure available, but was also the best representative structure of a HuR “closed” form available. Receptor structure was then prepared through the Protein Preparation Wizard, also implemented in Maestro, and the OPLS-2005 force field. Water molecules and residual crystallographic buffer components were removed, missing side chains were built using the Prime module, hydrogen atoms were added, side chains protonation states at pH 7.0 were assigned and, finally, minimization was performed until the RMSD of all the heavy atoms was within 0.3 Å of the crystallographically determined positions. In both cases, the binding pocket was identified by placing a cube centered in proximity of the “hinge” loop between the RRM1 and RRM2 domains. Docking calculations were performed as following. Docking with Glide was carried out in extra-precision (XP) mode, using GlideScore for ligand ranking. The inner box size was chosen to be 40 Å in all directions and the size of the outer box was set by choosing a threshold length for the ligand size to be docked of 30 Å. A maximum of 100000 poses per ligand was set to pass to the grid refinement calculation and the best 10000 poses were kept for the energy minimization step. The maximum number of poses per ligand to be outputted was set to 10. In the case of docking with Autodock, the ligand and receptor structures were first converted to AD4 format files, adopting the Gasteiger-Marsili partial charges, via AutoDockTools⁵⁵. The box size was set to have 117x125x127 points in the three-dimensional space with a Grid spacing of 0.481 Å per point using AutoGrid 4.2. A hundred independent runs of the Lamarckian genetic algorithm local search (GALS) method per docking calculation were performed, by applying a threshold of maximum 10 million energy evaluations per run. The rest of the docking parameters was set as default. Docking conformations were clustered on the basis of their RMSD (tolerance = 2.0 Å) and

were ranked according to the AutoDock scoring function. In both cases, the box size was chosen so as to encompass the whole RNA binding surface of HuR.

Molecular dynamics simulation and analysis

The best ranked HuR-**6a** complexes, as issuing from the docking calculations, were submitted to MD simulations with NAMD⁵⁷, using the ff99SBildn Amber force field parameters^{58,59}, for protein and the parameters recently developed by Allnér and co-workers for ions⁶⁰. Parameters for **6a** were generated in two steps. Initially, charges were computed using the restrained electrostatic potential (RESP) fitting procedure⁶¹. The ESP was first calculated by means of the Gaussian09 package⁶² using a 6-31G* basis set at Hartree-Fock level of theory, and then the RESP charges were obtained by a two-stages fitting procedure using the program RED^{63,64}. Missing bond, angle, torsion and improper torsion angle parameters were then generated using Antechamber⁶⁵. The complex was then solvated in a 15 Å layer cubic water box using the TIP3P water model parameters. Neutrality was reached by adding five further Cl⁻ ions. The final system size was ~75 Å x 74 Å x 93 Å for a total number of atoms of ~48000. A 10 Å cutoff (switched at 8.0 Å) was used for atom pair interactions. The long-range electrostatic interactions were computed by means of the particle mesh Ewald (PME) method using a 1.0 Å grid spacing in periodic boundary conditions. The RATTLE algorithm was applied to constrain bonds involving hydrogen atoms, and thus a 2 fs integration time step could be used. The system was minimized in two stages: first, a 20000-step run was carried out with restraints on all the protein and ligand atoms (5 kcal/mol/Å²); then, a further 10000-step minimization was carried out by applying restraints on the ligand and C_α protein atoms only. A 2 ns NPT simulation at 200K and 1 atm was performed with restraints on all the protein atoms (5 kcal/mol/Å²), to adjust the volume of the simulation box, while preserving the minimized protein structure obtained in the previous steps. Afterwards, the system was slowly heated up to 300 K over a 3 ns period, gradually releasing the restraints (on the ligand and protein C_α atoms only) to

1 kcal/mol/Å² along the thermalization process. Subsequently, the system was equilibrated for 2 ns, gradually reducing the restraints to zero. Production runs were then performed under NPT conditions at 1 atm and 300 K. Each of the four simulations was extended up to 1.5 μs. MD trajectory visualization and RMSD analysis were performed by means of the VMD software ⁶⁶. All other analyses were performed using CPPTRAJ ⁶⁷ or in-house scripts exploiting the MDAnalysis library ⁶⁸. For analysis purposes, trajectories were fitted onto the β-sheet backbone atoms, owing to the HuR high overall flexibility, using the first frame as reference and then one frame each 100 ps. In the specific case of contact analysis only, we employed a different reference structure. Indeed, as the aim of the analysis was also to discriminate between contacts established in the HuR mRNA-bound conformation and possible contacts characteristic of new **6a**-induced conformations, we made a distinction between native and non-native contacts. A non-native contact, contrarily to a native contact, is a contact between atoms within a convenient distance (here 4 Å) that is not present in a certain reference structure (here the structure used for the docking calculations). Figures were generated using the UCSF-Chimera software package ⁶⁹ or in-house scripts with Matplotlib⁷⁰.

■ ASSOCIATED CONTENT

SupportingInformation. Synthetic protocols and analytical characterization (NMR and HPLC-MS) for final compounds **6b-6k**, **6n-6o**, **6q-6w** and for synthetic intermediates. Supporting Figures S1-S5 are respectively related to REMSA assays for aza-tanshinones, RMSD of MD simulations, and cell migration assays. Supporting Table 1, containing primary data from cell viability assays on aza-tanshinones.

■ AUTHOR INFORMATION

*Email: pierfausto.seneci@unimi.it. Phone: (+39)-02-50314060. Fax: (+39)-02-50314074.

*Email: lmarinel@unina.it. Phone: (+39)-081-679899.

*Email: alessandro.provenzani@unitn.it. Phone: (+39)-0461-283176.

Notes. The authors declare competing financial interest as the molecules herein reported are present in patents: Italian Patent 151367 and PCT/IB2017/053519

■ ACKNOWLEDGMENTS

Associazione Italiana per la Ricerca sul Cancro (AIRC) [17153 to A.P.]

■ ABBREVIATIONS USED

CAN, cerium ammonium nitrate; DDQ, 2,3-dichloro-5,6-dicyano-1,4-benzoquinone; DHTS, dihydrotanshinone I; DME, dimethoxyethane; DMF, dimethylformamide; EtOAc, ethyl acetate; FOS, function-oriented synthesis; HuR, human antigen R; IBX, 2-iodoxybenzoic acid; MeCN, acetonitrile; NMR, nuclear magnetic resonance; THF, tetrahydrofuran.

Bibliography

- (1) Keene, J. D. RNA Regulons: Coordination of Post-Transcriptional Events. *Nat. Rev. Genet.***2007**, 8 (7), 533–543.
- (2) Brennan, C. M.; Steitz, J. a. HuR and mRNA Stability. *Cell. Mol. Life Sci.***2001**, 58 (2), 266–277.
- (3) Latorre, E.; Carelli, S.; Raimondi, I.; D’Agostino, V.; Castiglioni, I.; Zucal, C.; Moro, G.; Luciani, A.; Ghilardi, G.; Monti, E.; Inga, A.; Di Giulio, A. M.; Gorio, A.; Provenzani, A. The Ribonucleic Complex HuR-MALAT1 Represses CD133 Expression and Suppresses Epithelial-Mesenchymal Transition in Breast Cancer. *Cancer Res.***2016**, 76 (9), 2626–2636.
- (4) Izquierdo, J. M. Hu Antigen R (HuR) Functions as an Alternative Pre-mRNA Splicing Regulator of Fas Apoptosis-Promoting Receptor on Exon Definition. *J. Biol. Chem.***2008**, 283 (27), 19077–19084.
- (5) Mukherjee, N.; Corcoran, D. L.; Nusbaum, J. D.; Reid, D. W.; Georgiev, S.; Hafner, M.; Ascano, M.; Tuschl, T.; Ohler, U.; Keene, J. D. Integrative Regulatory Mapping Indicates That the RNA-Binding Protein HuR Couples Pre-mRNA Processing and mRNA Stability. *Mol. Cell***2011**, 43 (3), 327–339.
- (6) Al-Ahmadi, W.; Al-Ghamdi, M.; Al-Haj, L.; Al-Saif, M.; Khabar, K. S. A. Alternative Polyadenylation Variants of the RNA Binding Protein, HuR: Abundance, Role of AU-Rich Elements and Auto-Regulation. *Nucleic Acids Res.***2009**, 37 (11), 3612–3624.
- (7) Lebedeva, S.; Jens, M.; Theil, K.; Schwanhäusser, B.; Selbach, M.; Landthaler, M.; Rajewsky, N. Transcriptome-Wide Analysis of Regulatory Interactions of the RNA-Binding Protein HuR. *Mol. Cell***2011**, 43 (3), 340–352.

- (8) Katsanou, V.; Papadaki, O.; Milatos, S.; Blackshear, P. J.; Anderson, P.; Kollias, G.; Kontoyiannis, D. L. HuR as a Negative Posttranscriptional Modulator in Inflammation. *Mol. Cell***2005**, *19* (6), 777–789.
- (9) Wang, W.; Caldwell, M. C.; Lin, S.; Furneaux, H.; Gorospe, M. HuR Regulates Cyclin A and Cyclin B1 mRNA Stability during Cell Proliferation. *EMBO J***2000**, *19*, 2340–2350.
- (10) Abdelmohsen, K.; Pullmann, R.; Lal, A.; Kim, H. H.; Galban, S.; Yang, X.; Blethrow, J. D.; Walker, M.; Shubert, J.; Gillespie, D. a; Furneaux, H.; Gorospe, M. Phosphorylation of HuR by Chk2 Regulates SIRT1 Expression. *Mol. Cell***2007**, *25* (4), 543–557.
- (11) Abdelmohsen, K.; Gorospe, M. Posttranscriptional Regulation of Cancer Traits by HuR. *Wiley Interdiscip. Rev. RNA***2010**, *1* (2), 214–229.
- (12) Levy, N. S.; Chung, S.; Furneaux, H.; Levy, A. P. Hypoxic Stabilization of Vascular Endothelial Growth Factor mRNA by the RNA-Binding Protein HuR. *J. Biol. Chem.***1998**, *273* (11), 6417–6423.
- (13) Tang, K.; Breen, E. C.; Wagner, P. D. Hu Protein R-Mediated Posttranscriptional Regulation of VEGF Expression in Rat Gastrocnemius Muscle. *Am. J. Physiol. Heart Circ. Physiol.***2002**, *283* (4), H1497-504.
- (14) Akool, E.-S.; Kleinert, H.; Hamada, F. M. A.; Abdelwahab, M. H.; Förstermann, U.; Pfeilschifter, J.; Eberhardt, W. Nitric Oxide Increases the Decay of Matrix Metalloproteinase 9 mRNA by Inhibiting the Expression of mRNA-Stabilizing Factor HuR. *Mol. Cell. Biol.***2003**, *23* (14), 4901–4916.
- (15) Wang, W.; Yang, X.; Cristofalo, V. J.; Holbrook, N. J.; Gorospe, M. Loss of HuR Is Linked to

Reduced Expression of Proliferative Genes during Replicative Senescence. *Mol. Cell. Biol.***2001**, *21* (17), 5889–5898.

- (16) Ishimaru, D.; Ramalingam, S.; Sengupta, T. K.; Bandyopadhyay, S.; Dellis, S.; Tholanikunnel, B. G.; Fernandes, D. J.; Spicer, E. K. Regulation of Bcl-2 Expression by HuR in HL60 Leukemia Cells and A431 Carcinoma Cells. *Mol. Cancer Res.***2009**, *7* (8), 1354–1366.
- (17) Abdelmohsen, K.; Lal, A.; Hyeon, H. K.; Gorospe, M. Posttranscriptional Orchestration of an Anti-Apoptotic Program by HuR. *Cell Cycle***2007**, *6* (11), 1288–1292.
- (18) Kafasla, P.; Skliris, A.; Kontoyiannis, D. L. Post-Transcriptional Coordination of Immunological Responses by RNA-Binding Proteins. *Nat. Immunol.***2014**, *15* (6), 492–502.
- (19) Atasoy, U.; Watson, J.; Patel, D.; Keene, J. D. ELAV Protein HuA (HuR) Can Redistribute between Nucleus and Cytoplasm and Is Upregulated during Serum Stimulation and T Cell Activation. *J. Cell Sci***1998**, *111*, 3145–3156.
- (20) Galbán, S.; Kuwano, Y.; Pullmann, R.; Martindale, J. L.; Kim, H. H.; Lal, A.; Abdelmohsen, K.; Yang, X.; Dang, Y.; Liu, J. O.; Lewis, S. M.; Holcik, M.; Gorospe, M. RNA-Binding Proteins HuR and PTB Promote the Translation of Hypoxia-Inducible Factor 1alpha. *Mol. Cell. Biol.***2008**, *28* (1), 93–107.
- (21) Zucal, C.; D’Agostino, V.; Loffredo, R.; Mantelli, B.; Thongon, N.; Lal, P.; Latorre, E.; Provenzani, A. Targeting the Multifaceted HuR Protein, Benefits and Caveats. *Curr. Drug Targets***2015**.
- (22) Christensen, M. K.; Erichsen, K. D.; Olesen, U. H.; Tjørnelund, J.; Fristrup, P.; Thouggaard, A.; Nielsen, S. J.; Sehested, M.; Jensen, P. B.; Loza, E.; Kalvinsh, I.; Garten, A.; Kiess, W.; Björkling,

F. Nicotinamide Phosphoribosyltransferase Inhibitors, Design, Preparation, and Structure-Activity Relationship. *J. Med. Chem.***2013**, *56* (22), 9071–9088.

- (23) Wang, H.; Zeng, F.; Liu, Q.; Liu, H.; Liu, Z.; Niu, L.; Teng, M.; Li, X. The Structure of the ARE-Binding Domains of Hu Antigen R (HuR) Undergoes Conformational Changes during RNA Binding. *Acta Crystallogr. D. Biol. Crystallogr.***2013**, *69* (Pt 3), 373–380.
- (24) D'Agostino, V. G.; Lal, P.; Mantelli, B.; Tiedje, C.; Zucal, C.; Thongon, N.; Gaestel, M.; Latorre, E.; Marinelli, L.; Seneci, P.; Amadio, M.; Provenzani, A. Dihydrotanshinone-I Interferes with the RNA-Binding Activity of HuR Affecting Its Post-Transcriptional Function. *Sci. Rep.***2015**, *5*, 16478.
- (25) Zhou, L.; Zuo, Z.; Chow, M. S. S. Danshen: An Overview of Its Chemistry, Pharmacology, Pharmacokinetics, and Clinical Use. *J. Clin. Pharmacol.***2005**, *45* (12), 1345–1359.
- (26) Wilson, R. M.; Danishefsky, S. J. Small Molecule Natural Products in the Discovery of Therapeutic Agents: The Synthesis Connection. *J. Org. Chem.***2006**, *71* (22), 8329–8351.
- (27) Wender, P. A.; Quiroz, R. V.; Stevens, M. C. Function through Synthesis-Informed Design. *Acc. Chem. Res.***2015**, *48* (3), 752–760.
- (28) Crane, E. A.; Gademann, K. Capturing Biological Activity in Natural Product Fragments by Chemical Synthesis. *Angew. Chemie Int. Ed.***2016**, *55* (12), 3882–3902.
- (29) Cheng, Y.-C.; Liou, J.-P.; Kuo, C.-C.; Lai, W.-Y.; Shih, K.-H.; Chang, C.-Y.; Pan, W.-Y.; Tseng, J. T.; Chang, J.-Y. MPT0B098, a Novel Microtubule Inhibitor That Destabilizes the Hypoxia-Inducible Factor-1 α mRNA through Decreasing Nuclear-Cytoplasmic Translocation of RNA-Binding Protein HuR. *Mol. Cancer Ther.***2013**, *12* (7), 1202–1212.

- (30) Fujiwara, Y.; Domingo, V.; Seiple, I. B.; Gianatassio, R.; Del Bel, M.; Baran, P. S. Practical C-H Functionalization of Quinones with Boronic Acids. *J. Am. Chem. Soc.***2011**, *133* (10), 3292–3295.
- (31) Frigerio, M.; Santagostino, M.; Sputore, S. A User-Friendly Entry to 2-Iodoxybenzoic Acid (IBX). *J. Org. Chem.***1999**, *64*, 4537-4538.
- (32) Dickschat, A.; Studer, A. Radical Addition of Arylboronic Acids to Various Olefins under Oxidative Conditions. *Org. Lett.***2010**, *12* (18), 3972–3974.
- (33) Lee, J.; Snyder, J. K. Ultrasound-Promoted Cycloadditions in the Synthesis of Salvia Miltiorrhiza Abietanoid O-Quinones. *J. Org. Chem.***1990**, *55* (17), 4995–5008.
- (34) D'Agostino, V. G.; Adami, V.; Provenzani, A. A Novel High Throughput Biochemical Assay to Evaluate the HuR Protein-RNA Complex Formation. *PLoS One***2013**, *8* (8), e72426.
- (35) Eglen, R. M.; Reisine, T.; Roby, P.; Rouleau, N.; Illy, C.; Bossé, R.; Bielefeld, M. The Use of AlphaScreen Technology in HTS: Current Status. *Curr. Chem. Genomics***2008**, *1*, 2–10.
- (36) Massignan, T.; Cimini, S.; Stincardini, C.; Cerovic, M.; Vanni, I.; Elezgarai, S. R.; Moreno, J.; Stravalaci, M.; Negro, A.; Sangiovanni, V.; Restelli, E.; Riccardi, G.; Gobbi, M.; Castilla, J.; Borsello, T.; Nonno, R.; Biasini, E. A Cationic Tetrapyrrole Inhibits Toxic Activities of the Cellular Prion Protein. *Sci. Rep.***2016**, *6* (1), 23180.
- (37) Latorre, E.; Castiglioni, I.; Gatto, P.; Carelli, S.; Quattrone, A.; Provenzani, A. Loss of Protein Kinase C δ /HuR Interaction Is Necessary to Doxorubicin Resistance in Breast Cancer Cell Lines. *J. Pharmacol. Exp. Ther.***2014**, *349* (1), 99–106.
- (38) Lal, P.; Cerofolini, L.; D'Agostino, V. G.; Zucal, C.; Fuccio, C.; Bonomo, I.; Dassi, E.; Giuntini, S.; Di Maio, D.; Vishwakarma, V.; Preet, R.; Williams, S. N.; Fairlamb, M. S.; Munk, R.;

Lehrmann, E.; Abdelmohsen, K.; Elezgarai, S. R.; Luchinat, C.; Novellino, E.; Quattrone, A.; Biasini, E.; Manzoni, L.; Gorospe, M.; Dixon, D. A.; Seneci, P.; Marinelli, L.; Fragai, M.; Provenzani, A. Regulation of HuR Structure and Function by Dihydrotanshinone-I. *Nucleic Acids Res.***2017**, 1–14.

- (39) Mujo, A.; Lixa, C.; Carneiro, L. A. M.; Anobom, C. D.; Almeida, F. C.; Pinheiro, A. S. ¹H, ¹⁵N and ¹³C Resonance Assignments of the RRM1 Domain of the Key Post-Transcriptional Regulator HuR. *Biomol. NMR Assign.***2014**, 1–4.
- (40) Benoit, R. M.; Meisner, N.-C.; Kallen, J.; Graff, P.; Hemmig, R.; Cèbe, R.; Ostermeier, C.; Widmer, H.; Auer, M. The X-Ray Crystal Structure of the First RNA Recognition Motif and Site-Directed Mutagenesis Suggest a Possible HuR Redox Sensing Mechanism. *J. Mol. Biol.***2010**, 397 (5), 1231–1244.
- (41) Sigurdardottir, A. G.; Winter, A.; Sobkowicz, A.; Fragai, M.; Chirgadze, D.; Ascher, D. B.; Blundell, T. L.; Gherardi, E. Exploring the Chemical Space of the Lysine-Binding Pocket of the First Kringle Domain of Hepatocyte Growth Factor/scatter Factor (HGF/SF) Yields a New Class of Inhibitors of HGF/SF-MET Binding. *Chem. Sci.***2015**, 6 (11), 6147–6157.
- (42) Nasti, R.; Rossi, D.; Amadio, M.; Pascale, A.; Unver, M. Y.; Hirsch, A. K. H.; Collina, S. Compounds Interfering with Embryonic Lethal Abnormal Vision (ELAV) Protein?RNA Complexes: An Avenue for Discovering New Drugs. *J. Med. Chem.***2017**, acs.jmedchem.6b01871.
- (43) Blanco, F. F.; Preet, R.; Aguado, A.; Vishwakarma, V.; Stevens, L. E.; Vyas, A.; Padhye, S.; Xu, L.; Weir, S. J.; Anant, S.; Meisner-Kober, N.; Brody, J. R.; Dixon, D. A. Impact of HuR Inhibition by the Small Molecule MS-444 on Colorectal Cancer Cell Tumorigenesis. *Oncotarget***2016**.

- (44) Wu, X.; Lan, L.; Wilson, D. M.; Marquez, R. T.; Tsao, W.; Gao, P.; Roy, A.; Turner, B. A.; McDonald, P.; Tunge, J. a; Rogers, S. a; Dixon, D. a.; Aubé, J.; Xu, L. Identification and Validation of Novel Small Molecule Disruptors of HuR-mRNA Interaction. *ACS Chem. Biol.***2015**, 150309150728009.
- (45) Lang, M.; Berry, D.; Passecker, K.; Mesteri, I.; Bhujju, S.; Ebner, F.; Sedlyarov, V.; Evstatiev, R.; Dammann, K.; Loy, A.; Kuzyk, O.; Kovarik, P.; Khare, V.; Beibel, M.; Roma, G.; Meisner-kober, N.; Gasche, C. HuR Small-Molecule Inhibitor Elicits Differential Effects in Adenomatosis Polyposis and Colorectal Carcinogenesis. **2017**, No. 14, 1–16.
- (46) Wu, X.; Lan, L.; Wilson, D. M.; Marquez, R. T.; Tsao, W.-C.; Gao, P.; Roy, A.; Turner, B. A.; McDonald, P.; Tunge, J. A.; Rogers, S. A.; Dixon, D. A.; Aubé, J.; Xu, L. Identification and Validation of Novel Small Molecule Disruptors of HuR-mRNA Interaction. *ACS Chem. Biol.***2015**.
- (47) Zhang, Y.; Jiang, P.; Ye, M.; Kim, S. H.; Jiang, C.; Lü, J. Tanshinones: Sources, Pharmacokinetics and Anti-Cancer Activities. *Int. J. Mol. Sci.***2012**, 13 (10), 13621–13666.
- (48) Pathak, R.; Nhlapo, J. M.; Govender, S.; Michael, J. P.; van Otterlo, W. A. L.; de Koning, C. B. A Concise Synthesis of Novel Naphtho[a]carbazoles and Benzo[c]carbazoles. *Tetrahedron***2006**, 62 (12), 2820–2830.
- (49) Leboho, T. C.; Michael, J. P.; van Otterlo, W. A. L.; van Vuuren, S. F.; de Koning, C. B. The Synthesis of 2- and 3-Aryl Indoles and 1,3,4,5-tetrahydropyrano[4,3-B]indoles and Their Antibacterial and Antifungal Activity. *Bioorg. Med. Chem. Lett.***2009**, 19 (17), 4948–4951.
- (50) Dong, J.; Feldmann, G.; Huang, J.; Wu, S.; Zhang, N.; Comerford, S. A.; Gayyed, M. F.; Anders,

R. A.; Maitra, A.; Pan, D. Elucidation of a Universal Size-Control Mechanism in *Drosophila* and Mammals. *Cell***2007**, *130* (6), 1120–1133.

- (51) Keene, J. D.; Komisarow, J. M.; Friedersdorf, M. B. RIP-Chip: The Isolation and Identification of mRNAs, microRNAs and Protein Components of Ribonucleoprotein Complexes from Cell Extracts. *Nat. Protoc.***2006**, *1* (1), 302–307.
- (52) Thongon, N.; Castiglioni, I.; Zucal, C.; Latorre, E.; D’Agostino, V.; Bauer, I.; Pancher, M.; Ballestrero, A.; Feldmann, G.; Nencioni, A.; Provenzani, A. The GSK3β Inhibitor BIS I Reverts YAP-Dependent EMT Signature in PDAC Cell Lines by Decreasing SMADs Expression Level. *Oncotarget***2016**, *7* (18), 26551–26566.
- (53) Sigurdardottir, A. G.; Winter, A.; Sobkowicz, A.; Fragai, M.; Chirgadze, D.; Ascher, D. B.; Blundell, T. L.; Gherardi, E. Exploring the Chemical Space of the Lysine-Binding Pocket of the First Kringle Domain of Hepatocyte Growth Factor/scatter Factor (HGF/SF) Yields a New Class of Inhibitors of HGF/SF-MET Binding.
- (54) V.S.d. Glide, LLC, New York. 2014.
- (55) Morris, G. M.; Huey, R.; Lindstrom, W.; Sanner, M. F.; Belew, R. K.; Goodsell, D. S.; Olson, A. J. AutoDock4 and AutoDockTools4: Automated Docking with Selective Receptor Flexibility. *J. Comput. Chem.***2009**, *30* (16), 2785–2791.
- (56) *V.S. Maestro*; LLC.
- (57) Phillips, J. C.; Braun, R.; Wang, W.; Gumbart, J.; Tajkhorshid, E.; Villa, E.; Chipot, C.; Skeel, R. D.; Kalé, L.; Schulten, K. Scalable Molecular Dynamics with NAMD. *J. Comput. Chem.***2005**, *26* (16), 1781–1802.

- (58) Cornell, W. D.; Cieplak, P.; Bayly, C. I.; Gould, I. R.; Merz, K. M.; Ferguson, D. M.; Spellmeyer, D. C.; Fox, T.; Caldwell, J. W.; Kollman, P. A. A Second Generation Force Field for the Simulation of Proteins, Nucleic Acids, and Organic Molecules. *J. Am. Chem. Soc.* **1995**, *117* (19), 5179–5197.
- (59) Lindorff-Larsen, K.; Piana, S.; Palmo, K.; Maragakis, P.; Klepeis, J. L.; Dror, R. O.; Shaw, D. E. Improved Side-Chain Torsion Potentials for the Amber ff99SB Protein Force Field. *Proteins Struct. Funct. Bioinforma.* **2010**, *78* (8), NA-NA.
- (60) Allnér, O.; Nilsson, L.; Villa, A. Magnesium Ion–Water Coordination and Exchange in Biomolecular Simulations. *J. Chem. Theory Comput.* **2012**, *8* (4), 1493–1502.
- (61) Bayly, C. I.; Cieplak, P.; Cornell, W.; Kollman, P. A. A Well-Behaved Electrostatic Potential Based Method Using Charge Restraints for Deriving Atomic Charges: The RESP Model. *J. Phys. Chem.* **1993**, *97* (40), 10269–10280.
- (62) *Gaussian 09, Revision B.01*; 2009.
- (63) Dupradeau, F.-Y.; Pigache, A.; Zaffran, T.; Savineau, C.; Lelong, R.; Grivel, N.; Lelong, D.; Rosanski, W.; Cieplak, P. The R.E.D. Tools: Advances in RESP and ESP Charge Derivation and Force Field Library Building. *Phys. Chem. Chem. Phys.* **2010**, *12* (28), 7821.
- (64) Vanquelef, E.; Simon, S.; Marquant, G.; Garcia, E.; Klimmerak, G.; Delepine, J. C.; Cieplak, P.; Dupradeau, F.-Y. R.E.D. Server: A Web Service for Deriving RESP and ESP Charges and Building Force Field Libraries for New Molecules and Molecular Fragments. *Nucleic Acids Res.* **2011**, *39* (Web Server issue), W511-517.
- (65) Wang, J.; Wang, W.; Kollman, P. A.; Case, D. A. Automatic Atom Type and Bond Type

Perception in Molecular Mechanical Calculations. *J. Mol. Graph. Model.* **2006**, 25 (2), 247–260.

- (66) Humphrey, W.; Dalke, A.; Schulten, K. VMD: Visual Molecular Dynamics. *J. Mol. Graph.* **1996**, 14 (1), 33–38, 27–28.
- (67) Roe, D. R.; Cheatham, T. E. PTRAJ and CPPTRAJ: Software for Processing and Analysis of Molecular Dynamics Trajectory Data. *J. Chem. Theory Comput.* **2013**, 9 (7), 3084–3095.
- (68) Michaud-Agrawal, N.; Denning, E. J.; Woolf, T. B.; Beckstein, O. MDAAnalysis: A Toolkit for the Analysis of Molecular Dynamics Simulations. *J. Comput. Chem.* **2011**, 32 (10), 2319–2327.
- (69) Pettersen, E. F.; Goddard, T. D.; Huang, C. C.; Couch, G. S.; Greenblatt, D. M.; Meng, E. C.; Ferrin, T. E. UCSF Chimera--a Visualization System for Exploratory Research and Analysis. *J. Comput. Chem.* **2004**, 25 (13), 1605–1612.
- (70) Matplotlib v2.0.2. 2017.

TOC

